Journal of Structural Geology, Vol. 8, Nos. 3/4, pp. 341 to 360, 1986
Printed in Great Britain

0191-8141/86 $03.00 + 0.00

Deformation within foreland thrust sheets by populations of minor faults

STEVEN WOJTAL

Department of Geology, Oberlin College, Oberlin, Ohio, U.S.A.

(*Received* 18 *July* 1984; *accepted in revised form* 16 *September* 1985)

Abstract—The dominant deformation mechanism within foreland thrust sheets is the displacement of blocks of weakly deformed rock on discrete, mineral-coated minor faults. In highly deformed layers at the bases of three Southern Appalachian foreland sheets, such minor faults are members of families or populations of consistently oriented structures. The deformation style is similar in all three sheets. Rock nearest each thrust was shortened in the direction of sheet transport and thickened by a family of faults oriented at low angles to the thrusts. Rock further above each thrust experienced only the first of these two deformation stages. Statistical analyses of fault populations from these three sheets demonstrate that their deformation is quantitatively as well as qualitatively similar. Deformation due to movement on minor faults is statistically homogeneous at the scale of an outcrop in one of these sheets; strain due to minor faults can be measured in that sheet. A strain profile across this sheet is similar to strain profiles across continuously deformed sheets from internal portions of mountain belts, suggesting that their responses to emplacement are similar.

INTRODUCTION

CHARACTERIZING strain in foreland thrust sheets is often problematic. Twinned calcite strain measurements indicate that shortening subparallel to transport is common within the main body of foreland sheets, that the principal directions of strain change systematically near thrusts, and that minor faults and folds have pronounced effects on local orientations and magnitudes of principal strains (Spang & Brown 1981, Allmendinger 1982, Groshong *et al.* 1984, Wiltschko *et al.* 1985). Twinned calcite strain measurements have limited utility, however. Reliable measurement of strain due to calcite twinning is restricted to mildly deformed carbonate rocks (Groshong 1972); deformation intensity near thrusts can be quite high. Likewise, calcite twinning often accounts for only a portion of the total finite strain in deformed carbonates. Deformed grain shapes, elliptical objects, or fossils are locally important sources of strain data for foreland sheets (Simon & Gray 1981, Beach 1982, Reks & Gray 1983). The applicability of more traditional strain measurement techniques in foreland sheets is also limited because indicators of homogeneous, continuous deformation are not present in all foreland sheets.

Arrays of minor faults are found in most foreland sheets, and it is clear that strains accrue as a result of movement on faults in those arrays (Reches 1978). In some cases, it is possible to estimate longitudinal strains due to minor faults by measuring the average change in length of a material line or surface cut by the faults or by calculating the bulk shortening due to slip on faults in a duplex (Boyer & Elliott 1982). As useful as these measurements are, knowing the change in length of one material line does not characterize the local strain state. The existence of an array of minor faults usually precludes explicit definition of finite strain or that component of fine strain due to fault movement. An explanation of the local relationship between minor faults and bulk deformation would significantly improve our understanding of how minor faults contribute to deforming thrust sheets. This is true even if this relationship can only be described qualitatively, particularly in those sheets where minor faults are the only deformation elements recognized.

Previous work on natural minor-fault arrays suggests plausible directions for further study. Arrays or populations of minor faults form a deformation fabric that is penetrative at the scale of a foreland sheet, and the geometry of this fabric is a reliable indicator of local deformation kinematics (Price 1967). Bielenstein (1969) used the systematic, plan-view variation in minor fault geometry to argue for diverging flow during emplacement of a thrust sheet in the Front Ranges of the Canadian Rockies. Similarly, Harris & Milici (1977) examined the geometry of minor faults in deformed zones adjacent to four Southern Appalachian thrusts. They argued that the features found near these thrusts are unusually well exposed but nonetheless typical examples of the thin deformed layers generated during the emplacement of foreland sheets. The systematic changes in minor fault geometry with distance from thrusts that they describe provide insight to foreland sheet emplacement in the same way that flow profiles in moving glaciers provide information on glacier mechanics (Wojtal 1982).

The aim of this contribution is to explore further how minor-fault arrays near foreland thrusts develop. Its focus is data collected in well-exposed sections above three Southern Appalachian thrusts first described by Harris & Milici (1977): the Cumberland Plateau (CP) thrust, the Hunter Valley (HV) thrust, and the Copper Creek (CC) thrust. These data show that minor-fault arrays reflect both the kinematics of deformation and local state of strain in these sheets, and they offer insight to the ways in which minor-fault arrays accommodate deformation in foreland sheets.

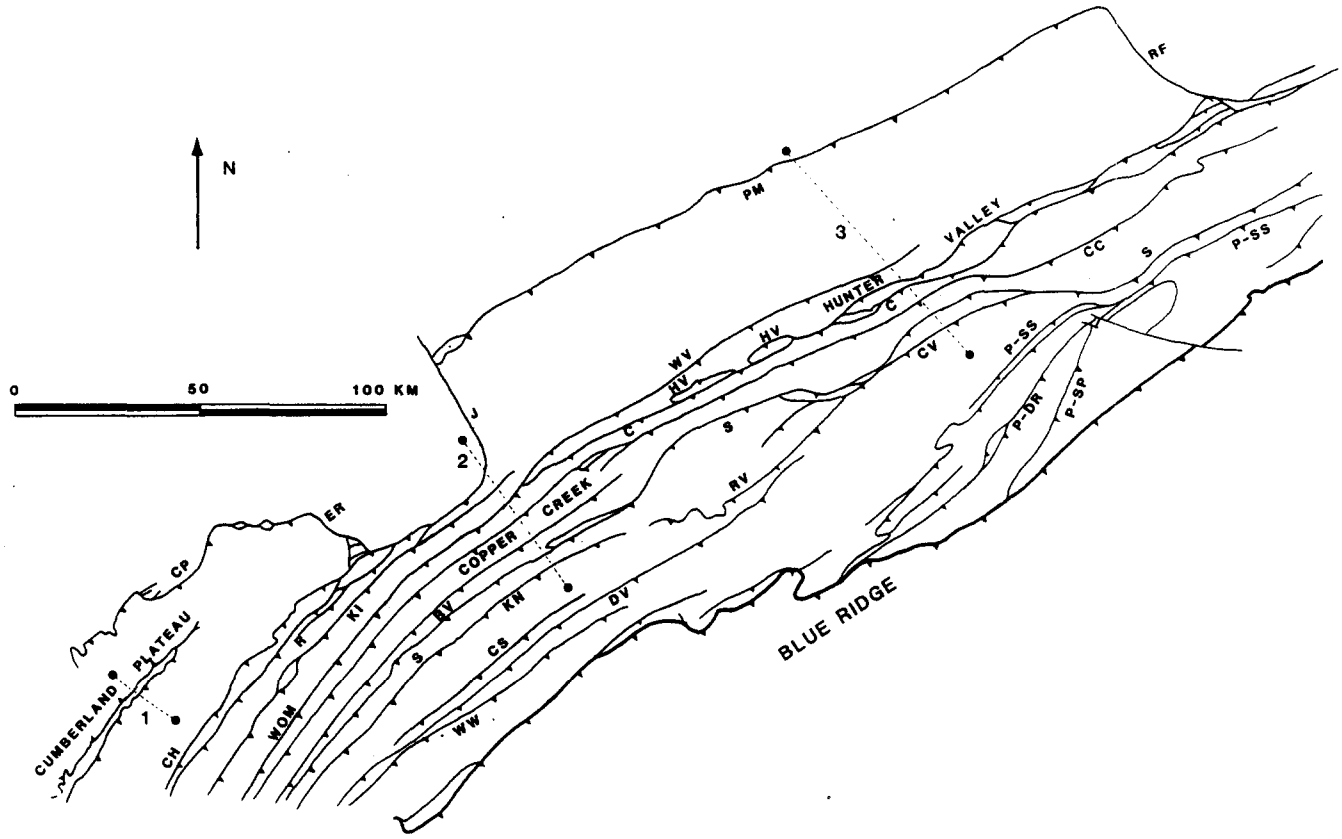

Fig. 1. Generalized map of Southern Appalachian thrust belt, redrawn from Rodgers (1970) and Roeder *et al.* (1978). BV, Beaver Valley thrust; C, Clinchport thrust; CC, Copper Creek thrust; CH, Chattanooga thrust; CP, Cumberland Plateau thrust; CS, Chestnut thrust; CV, Carter Valley thrust; DV, Dumplin Valley thrust; ER, Emory River fault; HV, Hunter Valley thrust; J, Jacksboro fault; KI, Kingston thrust; KN, Knoxville thrust; PM, Pine Mountain thrust; P-SP, P-DR, P-SS, branches of the Pulaski thrust; R, Rockwood thrust; RF, Russell Fork fault; RV, Rocky Valley thrust; S, Saltville thrust; WOM, White Oak Mountain thrust; WV, Wallen Valley thrust. Numbers give location of sections in Fig. 2.

Each of the thrusts described here lies in the predominantly thrust-faulted foreland of the Southern Appalachians (Fig. 1). The CP thrust locally marks the boundary between undeformed sedimentary cover to the west–northwest and thrusted cover to the east–southeast (Fig. 2a). The large-scale geometry of the CP thrust is relatively simple; it climbs from a glide horizon in Cambrian strata to another glide horizon in Pennsylvanian strata (Milici 1963). Displacement on the CP thrust ranges from 1 to 2 km at exposures of the footwall ramp to less than 1 km along the upper glide horizon. The geometry and displacement of the CP thrust are such that the Pennsylvanian units above the thrust's upper glide horizon never traveled over a large footwall ramp. The deformed Pennsylvanian rocks described here indicate that minor fault arrays develop early in a thrust's history and are not necessarily related to transport over a footwall ramp. The HV and CC thrusts are two of several large thrusts in the central portion of the transported Valley and Ridge Province (Rodgers 1970, pp. 47–48, Diegel & Wojtal 1985). Displacements on these thrusts are of the order of 15 to 20 km, sufficient to bring rocks from the regional décollement to the surface. At the exposure of the HV thrust described here, Cambrian limestones, dolostones and shales in a hangingwall flat lie on a low angle footwall ramp in Devonian shales and siltstones (Fig. 2c). At the surface exposure of the CC thrust described here, a hangingwall flat in the Cambrian Rome Formation lies on a footwall flat in Ordovician limestones (Fig. 2b).

GEOMETRY AND STYLE OF DEFORMATION

The two far-traveled (HV and CC) sheets have well-developed cataclasites at their bases; the CP sheet does not. Likewise, rocks within 10 m of the HV and CC thrusts are cut by bedding-normal stylolites. In the sandstones at the base of the CC sheet, bedding-normal stylolites are rather rare; a thin section (2.5 cm × 4 cm) might contain two or three stylolites. Although bedding-normal stylolites are quite common in the carbonate arenites at the base of the HV sheet, they do not produce a mappable fabric in the rocks. Bedding-normal stylolites are not found in the rocks at the base of the CP sheet. Other than these differences, the deformation style is remarkably similar in these three sheets. The primary effect of emplacement in each sheet was the development of an array of mesoscopic faults.

This mesoscopic array of faults is accompanied by numerous microfaults in rocks within 10 m of each thrust. Offsets on microfaults are generally small (fractions of a mm), but they can be as large as 0.5 cm. It is difficult to quantify the deformation accommodated by

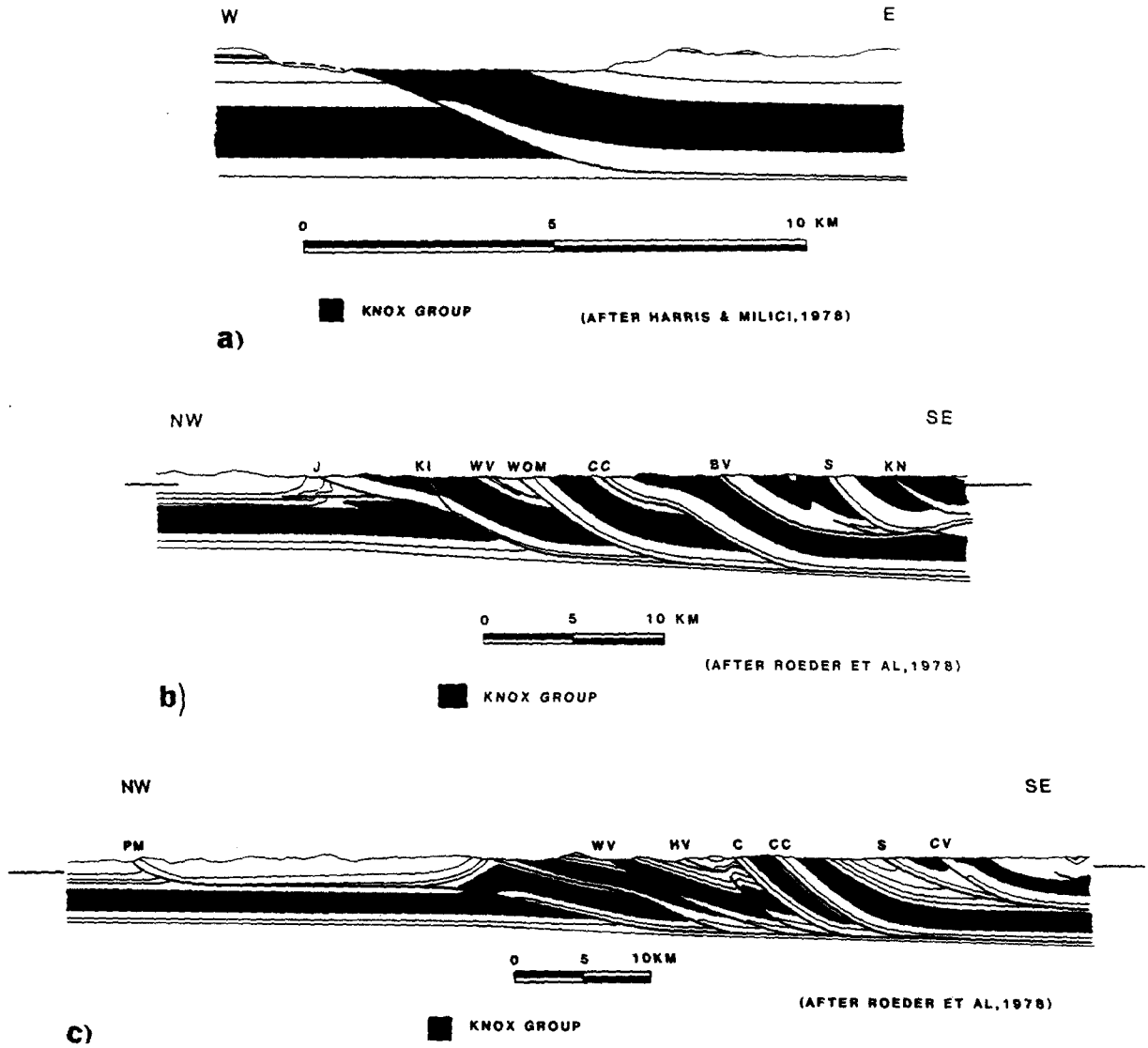

Fig. 2. (a) Cross-section of CP thrust at location 1, Fig. 1; redrawn from Harris & Milici (1977). (b) Cross-section of CC thrust at location 2, Fig. 1, redrawn from Roeder *et al.* (1978). (c) Cross-section of HV thrust at location 3, Fig. 1, redrawn from Roeder *et al.* (1978).

microfaults and stylolites, although they may locally account for large strains. Mesoscopic faulting may be accompanied by large homogeneous strains due to such deformation mechanisms without disrupting layering and without producing a mappable fabric (Cooper *et al.* 1983). In the remaining portions of these sheets, bedding normal stylolites and microfaults are confined to rock immediately adjacent to mesoscopic faults. Description of the deformation in these sheets, then, is contingent upon defining the characteristics of minor faults.

Rock a few millimetres away from most of the faults in these sheets is not measurably deformed, and individual faults are nearly always coated with a layer of fibrous mineral growth. Pressure-solution slip was the most important sliding mechanism operating on minor faults during deformation (Elliott 1976). Fibrous mineral coatings on faults are inferred to indicate the nature of fault movements during deformation (Durney & Ramsay 1973). This inference is corroborated in those cases where wall rock is measurably deformed; the local directions of shortening and elongations inferred from wall-rock deformation (subsidiary faults, mineral-filled extension veins and small-scale folds) are consistent with the direction of movement indicated by mineral fibers. Some minor faults, however, are coated by two or more layers of fibrous mineral growth in which the long axes of fibers have different orientations.

Individual minor faults from different parts of these sheets are indistinguishable, but the character of fault arrays, such as the spacing between faults in arrays and the general pattern of their offsets, change with position within a sheet. At comparable positions in these three sheets minor faults 'work together' in the same way, suggesting that populations or collections of minor faults, not individual faults, are the essential components of deformation in these sheets. Faults are not equally well developed in all lithologies in these sheets, but the local character of the minor-fault array correlates more strongly with position relative to the underlying thrust surfaces than with lithology. Similar minor faults occur in the rock beneath some of these thrusts, but no minor faults were found which cut and offset the thrust

surfaces. The minor-fault arrays described here are confined to rock above thrust surfaces.

Individual faults typically have one of three attitudes relative to the enveloping bedding: parallel to bedding, at low angles (≤45°) to bedding, or at high angles (≥45°) to bedding. Bedding-parallel faults are recognized by fibrous mineral growth on bedding surfaces. It is difficult to determine the amount of slip on most bedding-parallel faults, but a minimum estimate of the offset on bedding-parallel faults can be made in those cases where other faults are traced into or out of bedding-parallel faults. Demonstrated slip on bedding-parallel surfaces is as large as several meters.

Faults which cut bedding at low angles typically strike parallel to the underlying thrust's trend and have, or would have if extended, low-angle intersections with the thrusts. Fibrous mineral lineations on low-angle faults are usually oriented down their dip, and movement on these faults has produced reverse offsets of bedding. Low-angle faults are, then, contraction faults in the terminology of Norris (1958); Harris & Milici (1977) called these faults 'splays'. Offsets of several tens of meters on low-angle faults are observed. Low-angle faults nearest to the thrusts are generally sympathetic to thrusting. Farther from the thrusts, opposed-dip complexes are more common.

Faults which cut bedding at high angles usually strike either roughly parallel to the underlying thrust, or at 50–60° to the thrusts' trends. They have, or would have if extended, high-angle intersections with the underlying thrusts. Since most high-angle faults extend bedding, they are extension faults in Norris' (1958) terminology. Harris & Milici (1977) called high-angle faults either 'shear and rotational normal faults' or 'gravity normal faults', depending upon whether an individual high-angle fault lay between two low-angle faults or was isolated from low-angle faults. Where both low-angle faults and high-angle faults occur together, high-angle faults nearly always cut across low-angle faults. Wiltschko *et al.* (1985) recognized a similar pattern in the Pine Mountain thrust sheet. Where both kinds of high-angle faults are found, those which strike 50–60° to the underlying thrust generally crosscut those which strike parallel to thrust. Rakes of fibrous mineral lineations on high-angle faults range from 0 to 90°, with the attitude of the lineation on a particular high-angle fault a function of the fault's proximity to the thrust surface. Lineations on the regularly spaced high-angle faults near thrusts, both those with strikes parallel and oblique (50–60°) to the thrust's strike, typically have rakes from 0 to 45°. Movement on both types of high-angle faults near thrusts has produced both normal and reverse offsets of bedding, though normal offsets are far more common. Planar features with different original orientations, such as bedding and pre-existing low-angle faults, commonly have different offsets across these regularly spaced high-angle faults, indicating that slip was oblique to the fault's strike, and corroborating indications of fault movement given by mineral fibers on the fault surfaces. The regularly spaced high-angle faults near thrusts are, then, oblique-slip faults. Dip separations on oblique-slip high-angle faults are as large as 5 m, and the strike-parallel components of slip on many of these faults are larger than their dip-parallel components. High-angle faults farther from thrusts have a similar range of attitudes as those near thrusts. Most, however, have strikes parallel to the thrusts' strikes, down-dip lineations and normal offsets. High-angle faults farther from thrusts are neither so closely nor so regularly spaced as those near thrusts. Dip separations on high-angle faults farther from the thrusts are also as large as 5 m.

Folding occurred in some sedimentary units in these sheets, particularly in the CP and CC sheets. Most folds are anticlines or synclines associated with steps in minor fault surfaces. In other instances, folds appear to be 'drag' structures, apparently produced by shearing wall rock during movement on individual minor faults. Beds in the upright limbs of 'drag' folds are generally not affected by mesoscopic deformation, while those in the hinges are shortened by crenulations or small contraction faults. Beds in the overturned limbs of 'drag' folds were first shortened and later extended by extension veins or small extension faults. This arrangement of minor structures is consistent with migrating-hinge folding, where beds shortened in the neighborhood of a fold hinge are extended after the hinge moves farther from a minor fault as slip on that fault increases. Finally, there are rare instances in which minor faults can be traced up or down their dips into the cores of minor folds. Such fault-into-fold transitions could have developed as faults formed to empty the core of a tightening fold or as folds formed to accommodate deformation in the region surrounding the tip line of a minor fault (Ramsay 1974, Boyer & Elliott 1982). The three-dimensional exposure needed to distinguish between these two alternatives is lacking; two observations, however, suggest the latter interpretation is more likely. Simple parallel folds or simple kink folds without associated minor faults are not common; the initial stage of open folding expected in the first interpretation is not commonly found. Likewise, the cross-sectional area of rock affected by faults in fault-into-fold transitions is considerably larger than that affected by the folds. The faults appear to be the more important deformation elements in fault-into-fold transitions.

Since deformation in the neighborhood of each thrust is penetrative at a 'regional' scale, the techniques of structural analysis can be applied to the mesoscopic deformation elements (Turner & Weiss 1963, pp. 22–32). Stereographic projections of deformation elements from the regions near these thrusts indicate that the bulk deformation near each thrust has monoclinic symmetry (Figs. 3, 5 and 7). A plane oriented perpendicular to the thrust and containing the direction of sheet transport is a plane of mirror symmetry for bulk deformation. Annotated cross-sections of deformed regions adjacent to the CP, HV, and CC thrusts (Figs. 4, 6 and 8) are drawn parallel to the local symmetry planes. All faults with observed lengths ≥1 m are shown on the sections. Local

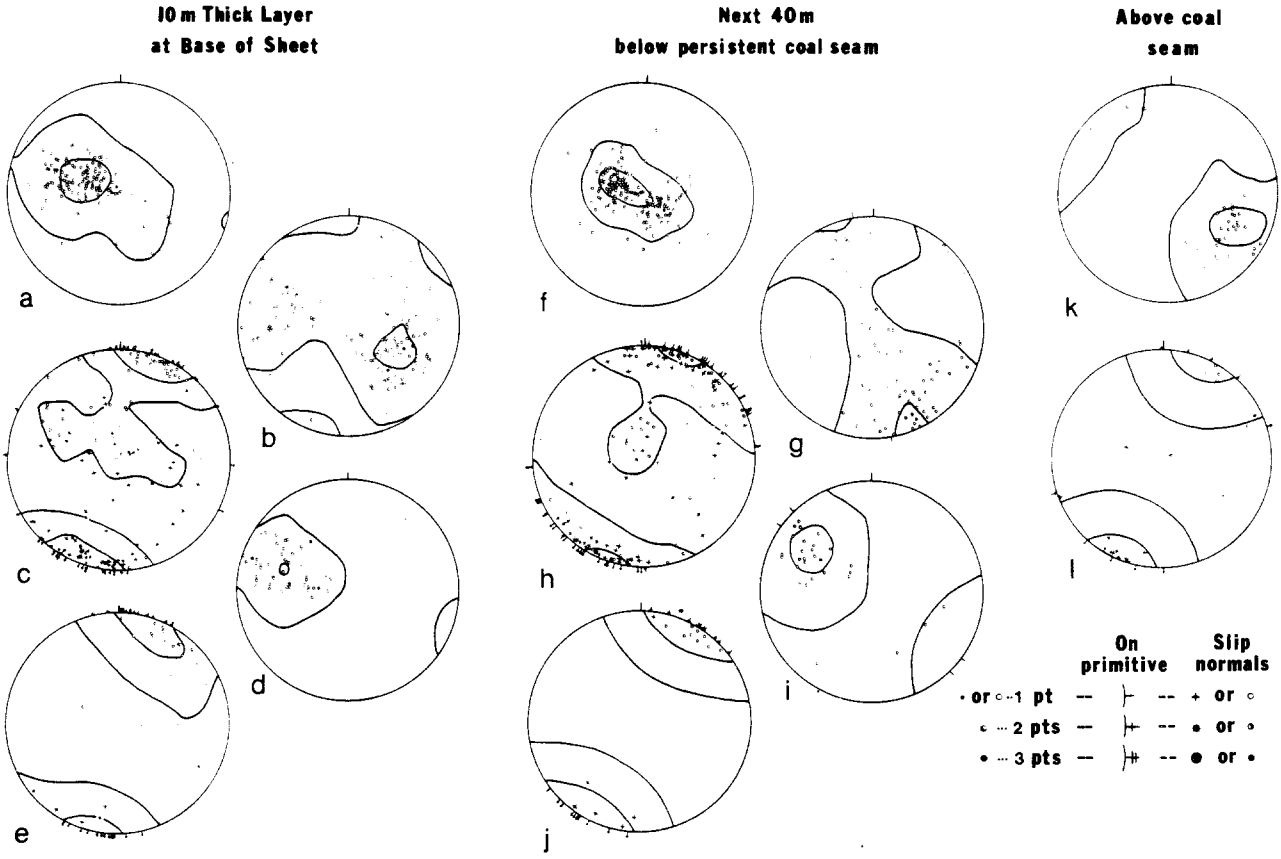

Fig. 3. Stereographic projections of structural data from CP sheet. Slip normals are assigned direction using an arbitrary 'right-hand' rule, where upward normal to fault parallels index finger, directed lineation parallels middle finger, and thumb points in positive direction along slip normal. Fold hinge lines assigned direction by convention similar to that defined by Hansen (1967); as fingers of right hand rotate from upright to overturned limb of fold, thumb points in positive direction along fold hinge. Directed line segments are plotted as circles if the line is directed from the primitive toward the center or crosses if the line is directed from the center toward the primitive. (a) Poles to low angle faults. $N = 138$. Contours are 1σ and 15σ. (b) Poles to high-angle faults. $N = 151$. Contours are 1σ and 10σ. (c) Directed slip normals to all faults. $N = 151$. Contours are 2σ and 10σ. (d) Poles to fold hinge surfaces. $N = 53$. Contours are 5σ and 18σ. (e) Fold hinge lines with sense of overturning. $N = 47$. Contours are 2σ and 8σ. (f) Poles to low-angle faults. $N = 166$. Contours are 5σ and 20σ. (g) Poles to high-angle faults. $N = 80$. Contours are 2σ and 9σ. (h) Directed slip normals to all faults. $N = 151$. Contours are 2σ and 15σ. (i) Poles to fold hinge surfaces. $N = 53$. Contours are 2σ and 10σ. (j) Fold hinge lines with sense of overturning. $N = 25$. Contours are 2σ and 10σ. (k) Poles to fault surfaces. $N = 37$. Contours are 3σ and 10σ. (l) Directed slip normals for faults. $N = 26$. Contours are 3σ and 7σ.

values of fault surface area per unit volume (S/V) for faults with observed lengths ≥ 1 m, measured using the technique outlined by Underwood (1970, pp. 54–58), are included in the annotation.

Offsets on low-angle faults are generally larger than those on high-angle faults. Offsets on both high- and low-angle faults near thrusts are generally larger than offsets on corresponding faults farther from thrusts. Likewise, measured S/V values for faults with observed lengths ≥ 1 m in each sheet are greatest in rock adjacent to thrusts. Curiously, the maximum S/V value in all three sheets is similar, about 1.0 m^{-1}. Fault S/V decreases irregularly with distance from the thrusts. Deformation intensity, as indicated by the magnitude of offsets on faults and by the values of fault S/V, is greatest near the thrusts. It drops off quickly with distance from the thrusts. The deformed layer at the base of the CP sheet is about 100 m thick; deformed layers at the bases of the HV and CC sheet are 300–400 m thick. Although there are differences in the degree of development of mesoscopic structures in these three sheets (Figs. 3–8), the kinds of structures in the sheets are the same. The sense of offset on minor faults, particularly those nearest to the thrusts, and the sense of overturning of folds indicate that structurally higher portions of each sheet were displaced farther toward the craton than structurally lower portions of the sheet. Likewise, a comparable sequence of events occurred in each sheet.

This sequence is apparent in the way minor structures are arranged above each thrust. At the top of each deformed layer, rock was shortened subparallel to transport and thickened by low-angle (contraction) faults only. Because many low-angle faults do not strike exactly parallel to the underlying thrust, they must move rock normal to transport (Fig. 9a). This movement normal to transport may contribute to the origin of the transverse extension faults found in some foreland sheets. Nearer to the HV and CC thrust and adjacent to the CP thrust, beds were first shortened subparallel to transport and thickened by low-angle faults and then cut by high-angle faults with strikes parallel to the thrust's strike. Oblique slips are the rule on these high-angle

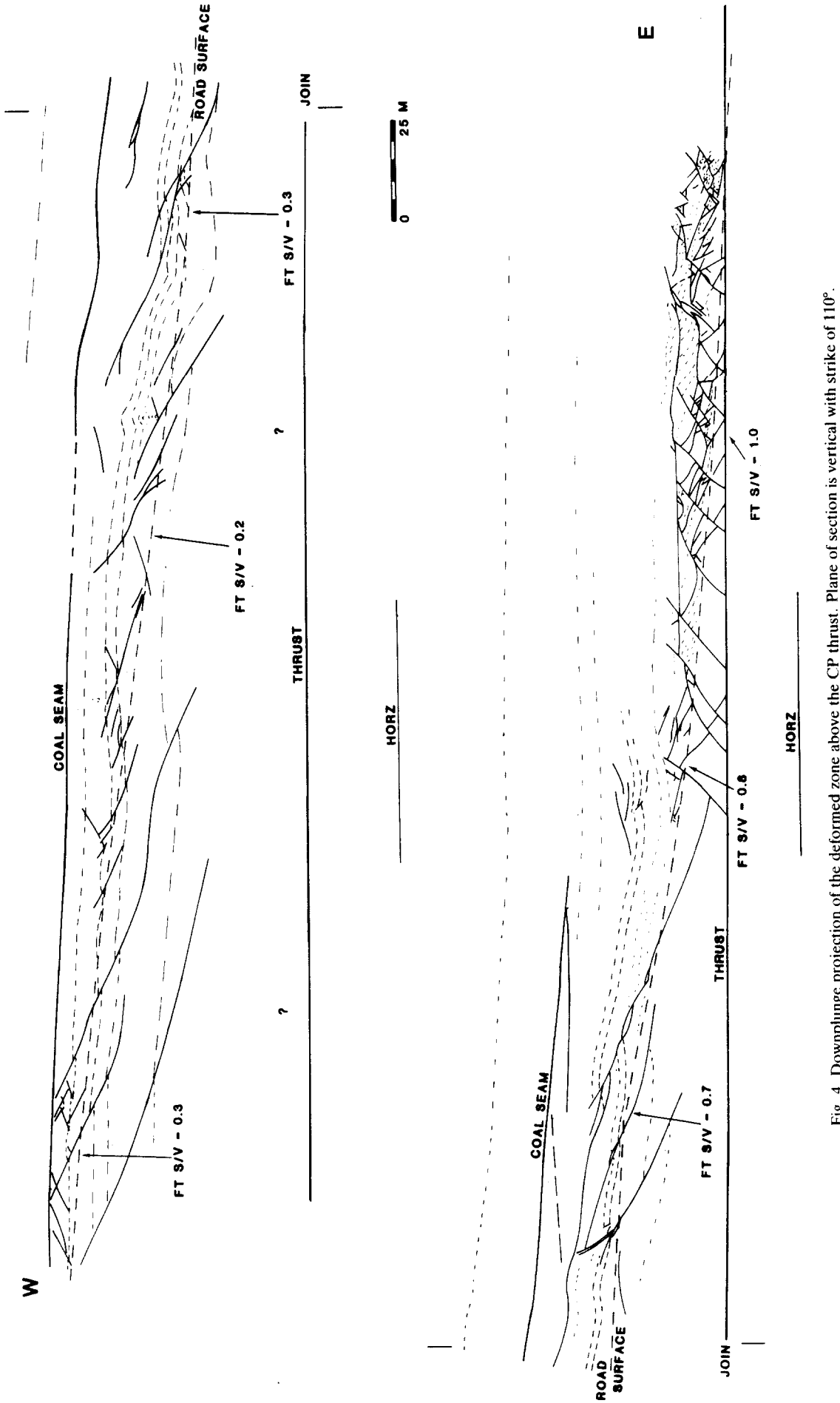

Fig. 4. Downplunge projection of the deformed zone above the CP thrust. Plane of section is vertical with strike of 110°. Structure above coal seam not shown.

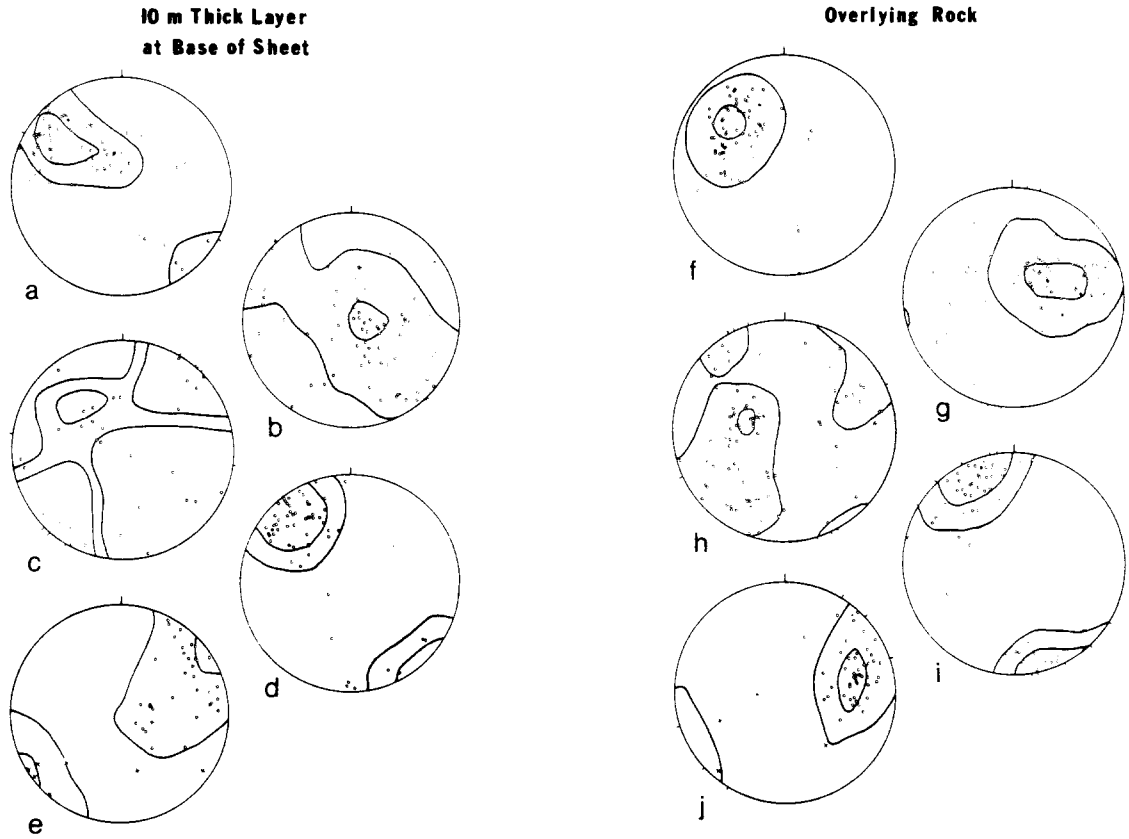

Fig. 5. Stereographic projections of structural data from the CC sheet. Points are plotted using conventions outlined for Fig. 3. (a) Poles to low-angle faults. $N = 75$. Contours are 5σ and 10σ. (b) Poles to high-angle faults. $N = 86$. Contours are 2σ and 8σ. (c) Directed slip normals to all faults. $N = 37$. Contours are 3σ and 4σ. (d) Poles to fold hinge surfaces. $N = 60$. Contours are 5σ and 10σ. (e) Fold hinge lines with sense of overturning. $N = 42$. Contours are 3σ and 8σ. (f) Poles to low angle faults. $N = 70$. Contours are 5σ and 15σ. (g) Poles to high angle faults. $N = 118$. Contours are 3σ and 10σ. (h) Directed slip normals to all faults. $N = 89$. Contours are 3σ and 8σ. (i) Poles to fold hinge surfaces. $N = 63$. Contours are 5σ and 10σ. (j) Fold hinge lines with sense of overturning. $N = 53$. Contours are 5σ and 12σ.

faults, with both down-dip (extensional) and strike-slip components to movement. These high-angle faults have extended layering parallel to transport and moved material normal to transport. This process occurred without altering the overall monoclinic symmetry of the deformation (Fig. 9b); its net result is flattening in the plane of the thrust surface. The transition from this zone of flattening to the overlying zone of shortening subparallel to transport only is exposed in the section above the CP thrust; oblique-slip high-angle faults lose offset upwards into drape folds here. The isolated high-angle faults found above this zone are normal-slip extension faults. Nearest the HV and CC thrusts, strata are cut by regularly spaced high-angle faults which strike either parallel or oblique to the underlying thrust's strike. Oblique-slip displacements are the rule on both sets of high-angle faults, with some component of down-dip, extensional movement common. The two sets of high-angle faults together move rock normal to transport and extend rock parallel to transport.

Both the zone of shortening and thickening followed by flattening and the zone of shortening and thickening alone are thicker in the two far-traveled sheets than in the CP sheet. Oblique-slip high-angle faults in the central portions of the deformed layers above the HV and CC thrusts cut through rock that once looked like the upper portion of the CP sheet. Rock that is shortened subparallel to transport and thickened only overlies this material. This pattern suggests that the deformed layer adjacent to a thrust thickens progressively during movement on the underlying thrust (Fig. 10).

The geometry of minor folds in the CP and CC sheets provides further support for the interpretation that structures developed progressively during sheet movement. Minor folds in both sheets have similar modes of occurrence, but their geometry is not identical. Hinge lines of minor folds from the CP sheet cluster about a line perpendicular to the local symmetry plane for deformation (Figs. 3e &j). Hinge lines of minor folds from the CC sheet lie along a plane that strikes parallel to the thrust and is inclined about 30° to the thrust (Fig. 11). Minor folds in the CC sheet are, nonetheless, consistently overturned to the NW, and they are symmetrically disposed about an upright plane containing the sheet's movement direction, the local symmetry plane for mesoscopic deformation elements. Data from the CP sheet indicate that transverse folds form early in a sheet's history. Subsequent flattening subparallel to the thrust could rotate such early folds into the orientations observed in the CC sheet if the direction of maximum elongation is subparallel to transport (Sanderson 1973). Comparable fold hinge geometries are observed in

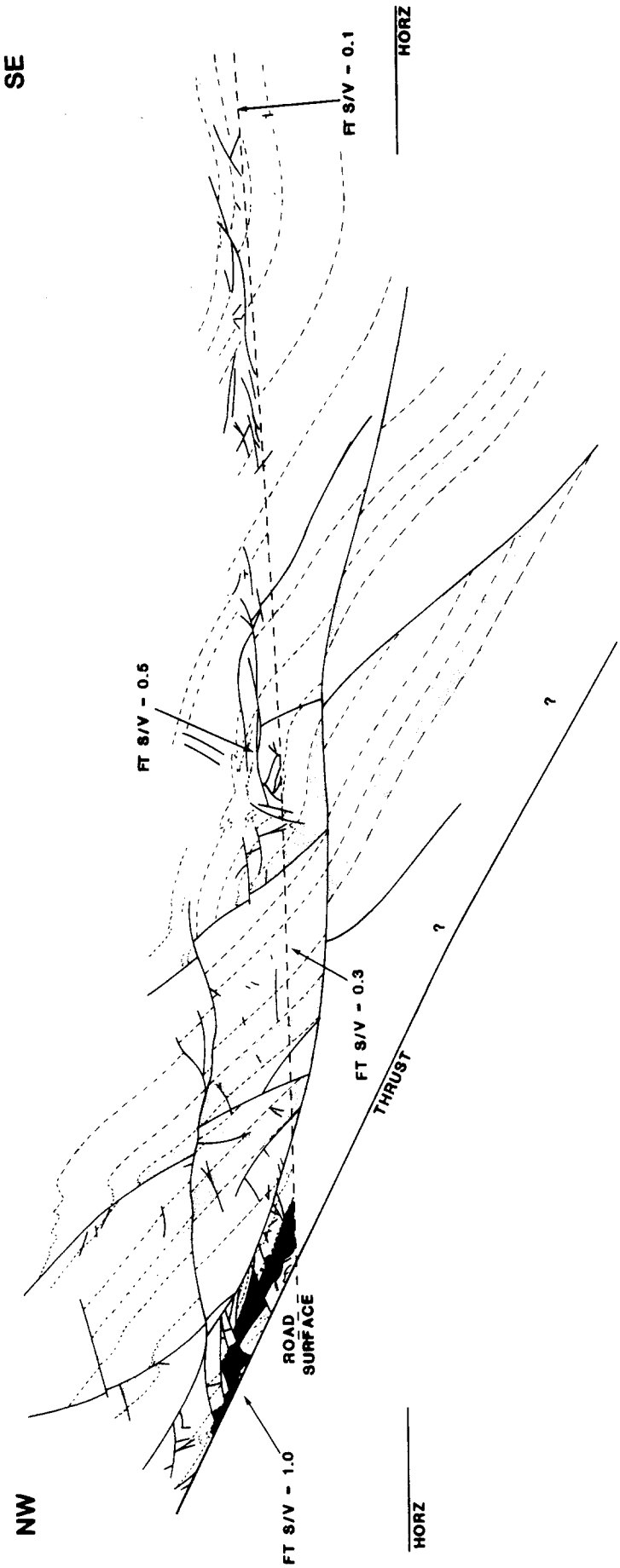

Fig. 6. Downplunge projection of deformed zone above the CC thrust. Plane of section is vertical with strike of 130°.

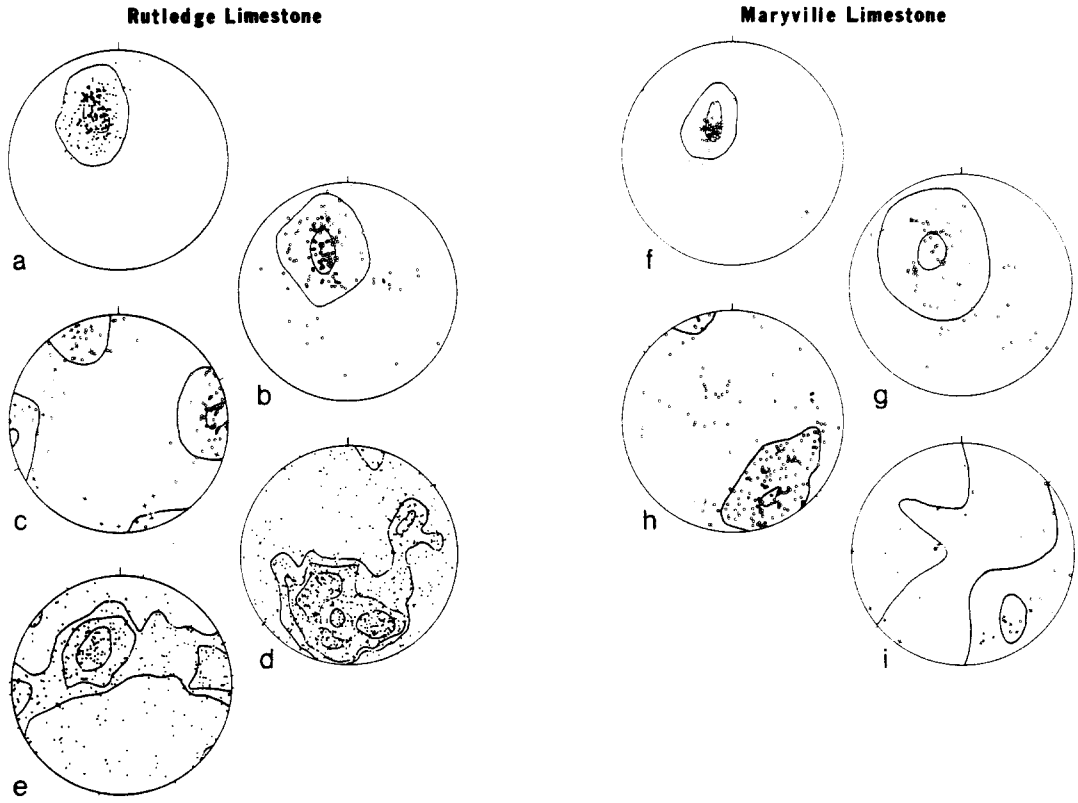

Fig. 7. Stereographic projections of structural data from the HV sheet. Points are plotted using conventions outlined for Fig. 3. (a) Poles to bedding. $N = 199$. Contours are 5σ and 30σ. (b) Poles to low-angle faults. $N = 150$. Contours are 5σ and 20σ. (c) Directed slip normals to low-angle faults. $N = 115$. Contours are 5σ and 12σ. (d) Poles to high-angle faults. $N = 680$. Contours are 3σ, 5σ, and 8σ. (e) Slip normals to high-angle faults. $N = 350$. Contours are 3σ, 5σ, and 10σ. (f) Poles to bedding. $N = 87$. Contours are 10σ and 20σ. (g) Poles to low-angle faults. $N = 77$. Contours are 3σ and 12σ. (h) Poles to high-angle faults. $N = 200$. Contours are 5σ and 18σ. (i) Slip normals to faults. $N = 40$ (31 directed or right-hand rule slip normals and 9 without directions). Contours are 2σ and 4σ.

minor folds from thrust sheets at several locations (Kvale 1953, Bryant & Reed 1969, Williams 1976). While the data cited come from sheets emplaced under conditions of higher metamorphic grade than those experienced by foreland sheets, this pattern is anticipated in the highly deformed portion of any thrust sheet.

FAULT POPULATION STATISTICS

The progressive nature of deformation near thrusts suggests that individual minor faults in a thrust sheet had unique histories. The collection of minor faults preserved near a thrust must include faults that initiated at different times, faults that accumulated slip at unique rates, and faults that ceased to be active at distinct times during emplacement. I can think of no reliable ways to examine individual minor faults and determine which factors governed their exact time of initiation, slip rate, or time of cessation of activity. Besides, these data are controlled by local perturbations in the overall deformation as well as the character of the overall deformation. The concerted activity of the population of minor faults, not the action of individual faults, produced the overall deformation in each sheet. This must be so. Either five (in the case of a general irrotational strain) or six (in the case of a general rotational strain) independent slip systems are needed to effect a homogeneous shape change (Reches 1978). More restrictive deformations, such as simple shear, require fewer independent slip systems, but in all cases the collective character of slip surfaces reflects the nature of the deformation better than the character of individual slip surfaces. The rate at which faults were initiated, their average tendency to remain active, and the rate at which faults ceased to be active were dictated by the overall deformation. Population statistics of this sort, if they can be determined, are more likely to reflect the factors that controlled deformation than the character of individual minor faults. They are, then, more reliable bases for comparing deformation in different sheets.

An analogous situation occurs in paleoecological studies focused on assessing the factors which control the birth, growth and death of once living organisms. The life history (absolute time of birth, size at all ages and absolute age at death) of an individual organism *per se* is less useful than the population's rates of recruitment (addition to the population), average growth and mortality. The dynamics of an organic population can be understood only when these population statistics are known, but these statistics can be fixed exactly only when life histories are known for all individuals in the population. On the other hand, size distributions for fossil assemblages are often and easily compiled. If the size distribution of a fossil assemblage is assumed to represent the age distribution of a death assemblage in a

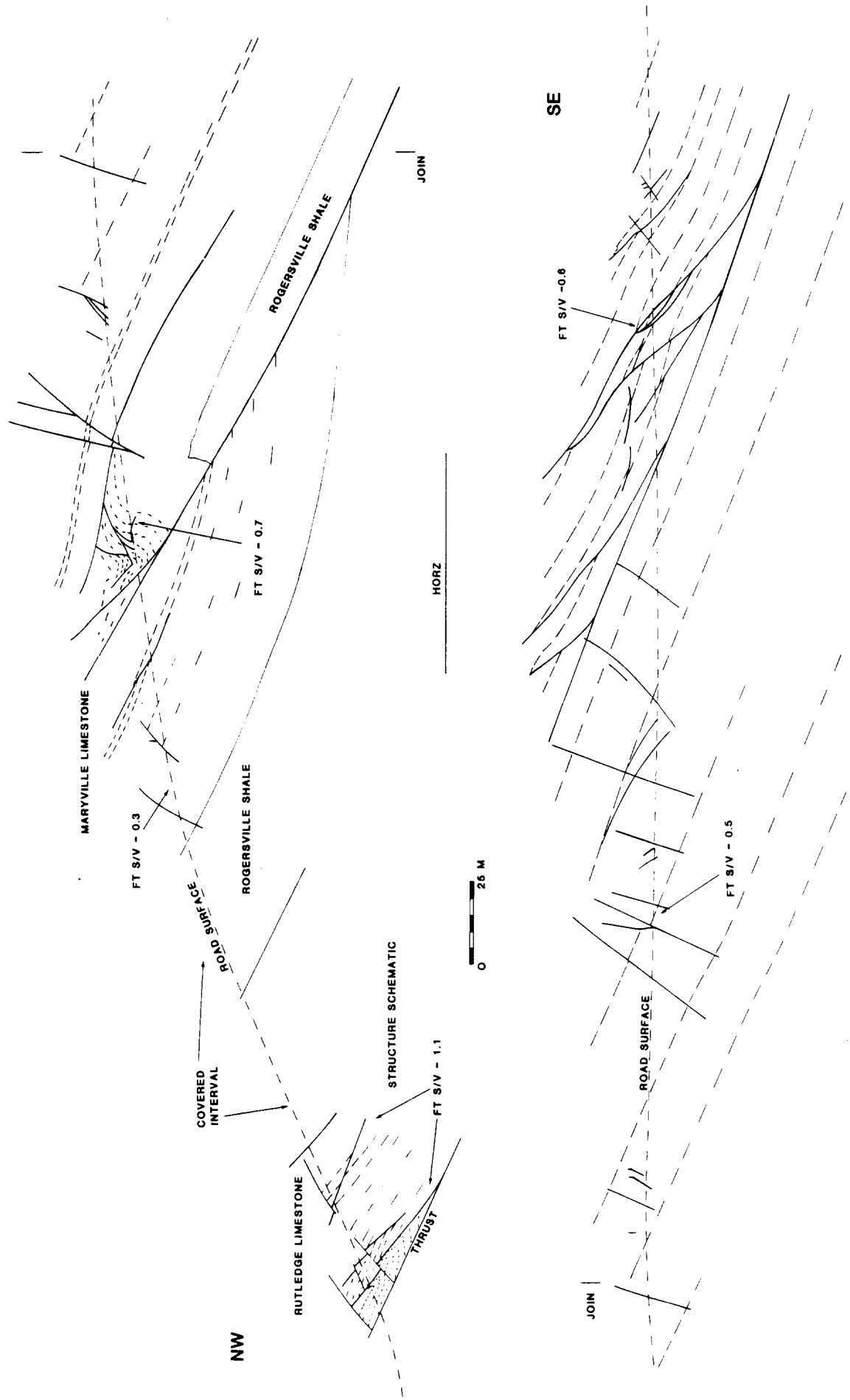

Fig. 8. Downplunge projection of deformed zone above the HV thrust. Plane of section dips 85° toward the bearing 250°.

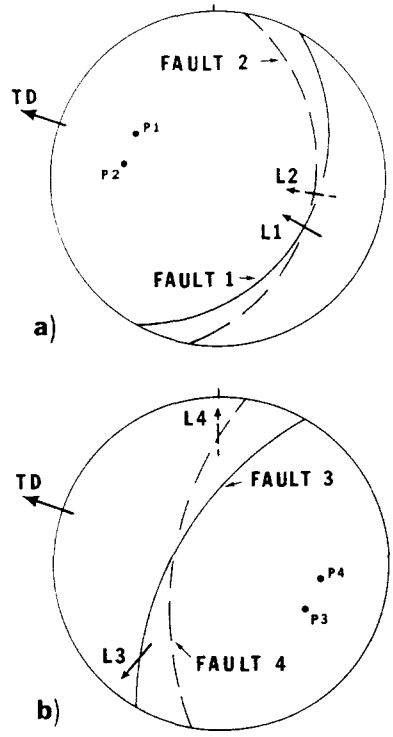

Fig. 9. (a) Lower hemisphere stereographic projection of low-angle faults 1 and 2 and poles to faults, P1 and P2. Since fault strikes are not strictly normal to transport direction (TD), displacement of hanging wall of fault 1 up L1 and hanging wall of fault 2 up L2 moves rock normal to transport. (b) Lower hemisphere projections of high-angle faults 3 and 4 and poles to faults, P3 and P4. Oblique-slip of hanging wall of fault 3 down L3 and hanging wall of fault 4 down L4 moves rock normal to TD as well as extending rock parallel to TD without altering symmetry of deformation. A similar diagram could be constructed for high-angle faults striking oblique to the thrust.

general way, it is possible to use the size distribution to estimate the living population's dynamic parameters (Craig & Oertel 1966, Hallam 1972).

Size distributions are most sensitive to changes in growth and mortality rates with age (Hallam 1972). Skewness toward small size results from a combination of low growth rates and high mortality rates for individuals of small size. Either increasing the growth rate or decreasing the mortality rate for small individuals will skew the size distribution toward large size. Without independent evidence on the relative size of the growth rate, it is impossible to determine whether this factor or the mortality rate controls the size distribution.

By applying statistical techniques to minor fault populations, data on the dynamics of discontinuous deformations can be garnered from collections of minor faults. The rate of fault initiation is really a recruitment rate for a dynamic fault population; the average tendency for individual faults to remain active is analogous to organisms' average growth rates. Likewise, the rate at which faults cease to be active is similar to the mortality rate of an organic population. I will consider slip on a fault to be as accurate a measure of the fault's maturity as the size of a fossil is a measure of its maturity. This is surely an approximation, but with this change in perspective, standard field observations can be used as a key to better understand the development of discontinuous deformation. The profiles above these three thrust faults are assumed to give representative samples of minor fault populations, with the collection of minor faults at a given structural level characteristic of the response of the sheet at that level. The fault population in a larger exposure of this structural level would have a greater number of faults but would have a similar 'size' distribution (distribution of displacement) as that found in a smaller exposure.

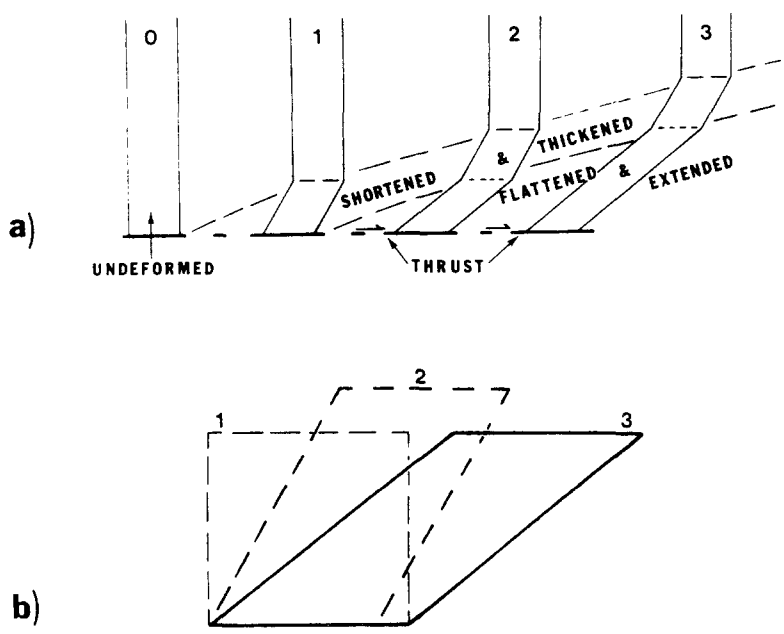

Fig. 10. (a) Schematic development of deformed zone at the base of a thrust sheet illustrating progressive thickening of deformed zone. (b) Minimum work simple shear of a perfectly plastic body, after Nadai (1963, pp. 98–99).

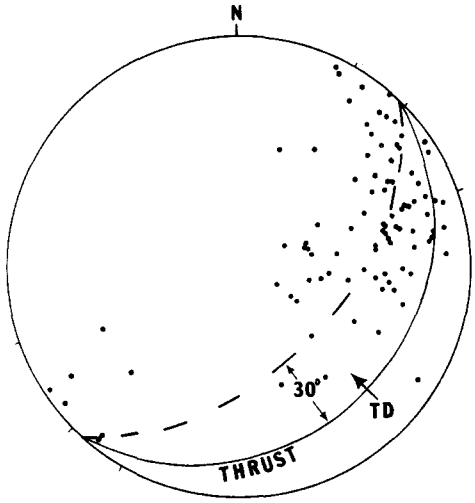

Fig. 11. Lower hemisphere equal-area projection of all fold hinge lines from the base of the CC sheet ($N = 95$); TD is the inferred transport direction. Fold hinge lines lie along a great circle inclined about 30° to the CC thrust.

A plot of frequency of occurrence of minor faults versus their displacements, called a *distribution diagram*, estimates the age-at-death distribution for a minor fault population. The fraction of the total number of minor faults, f_i, whose displacements fall within an arbitrary interval is plotted along the ordinate of the diagram. The value of the mean displacement of the interval, u_i, is plotted along its abscissa. The areas sampled at different structural levels in a sheet must have equal sizes to allow accurate measurement of the data for distribution diagrams, but the actual amount of rock exposed at different levels is rarely constant. Raw counts of faults in different displacement classes may not accurately portray the true population of faults within a sheet, and they must be corrected to remove any bias caused by different sizes of the sampled areas. One way to do so is to count faults in test areas centered in each structural level. This kind of sampling often yields numbers of faults that are too small to be useful. Instead, I have artificially made sampling areas of equal (large) size at different structural levels by multiplying each sampling area, and the raw counts from it, by a whole number which brings all sampling areas to a uniform large size. Each distribution diagram, then, has two total numbers of faults listed. N_t is the sum of the raw counts of faults in each section. N'_t is the total number of faults in a hypothetical section composed of sample areas of equal size at all structural levels. N'_t is greater than N_t in all cases. In all cases, the displacement value used is the minimum value needed to bring features on either side of the fault into continuity. As is the case with stereographic analysis of deformation elements, it is sensible to split the population into smaller collections with common structural significance. It is also useful to divide the value of the mean class displacement for each interval by the maximum displacement observed in the section to yield a set of normalized mean class displacements which range from zero to one. In this way, comparison of distribution diagrams from different sheets is facilitated. Survivorship curves for fault populations can be drawn using the data compiled for the distribution diagram.

Information on the relative importance of different displacement classes to the deformation is also available from a distribution diagram. The product of the mean displacement in an arbitrary class, u_i, and the frequency of occurrence of that class, f_i, gives the total displacement due to faults within that class

$$U_i = f_i u_i. \quad (1)$$

U_i is called the mean class displacement. The sum of mean class displacements for all classes is the total observed displacement, U_t

$$U_t = \Sigma_i U_i. \quad (2)$$

The ratio U_i/U_t is the fraction of the total observed displacement accomplished by faults in a particular displacement class. This ratio is a measure of the importance of faults with particular displacement values in the overall deformation (Elliott 1977).

The attitudes and offsets on minor faults in the sections across the CP and CC thrusts are well defined since the exposures from which these sections were derived run nearly perpendicular to the thrusts' strikes. A sufficient number of low-angle faults are present in each case to construct distribution diagrams for populations of low-angle faults (Figs. 12a and 13a). I have used offsets in the plane of section instead of true displacements. Since the strikes of low-angle faults in these sections are nearly perpendicular to the sections and sliding lineations on the faults are oriented nearly down the faults' dips, offsets measured in the plane of section closely approximate true displacements on these faults. The mean offset for each class is normalized by dividing its value by the largest offset measured on a low-angle fault in a sheet (14 m in the CP sheet and 48 m in the CC sheet).

Each plot is strongly skewed toward faults with small offset (≤50 cm). The distribution diagram for the CC sheet is also bimodal, with a peak for faults with very small offsets (≤25 cm) and a peak for faults with offsets of about 2 m. The origin and implications of the bimodal nature of this curve are discussed below. The extreme skewness of Figs. 12(a) and 13(a) suggests that small-offset faults accumulate offset relatively slowly and that many ceased to be active soon after initiation; low-angle faults had initially slow 'growth' rates and high attrition rates. On the other hand, if a fault 'survived' to achieve an offset of 1 m in the CP sheet or 2 m in the CC sheet, it was likely to have remained active during deformation and accumulate displacement relatively quickly. The relative sizes of attrition rates decreased and 'growth' rates increased as faults 'grew'. Survivorship curves are an alternative way of presenting these inferences (Figs. 12b and 13b).

By substituting the value of mean offset for each class, s_i, for u_i in equation (1), it is possible to calculate the mean class offset, S_i, for each class. Likewise, S_t, the sum of all S_i, is the total observed offset in these rocks. The relative importance of any offset class is represented

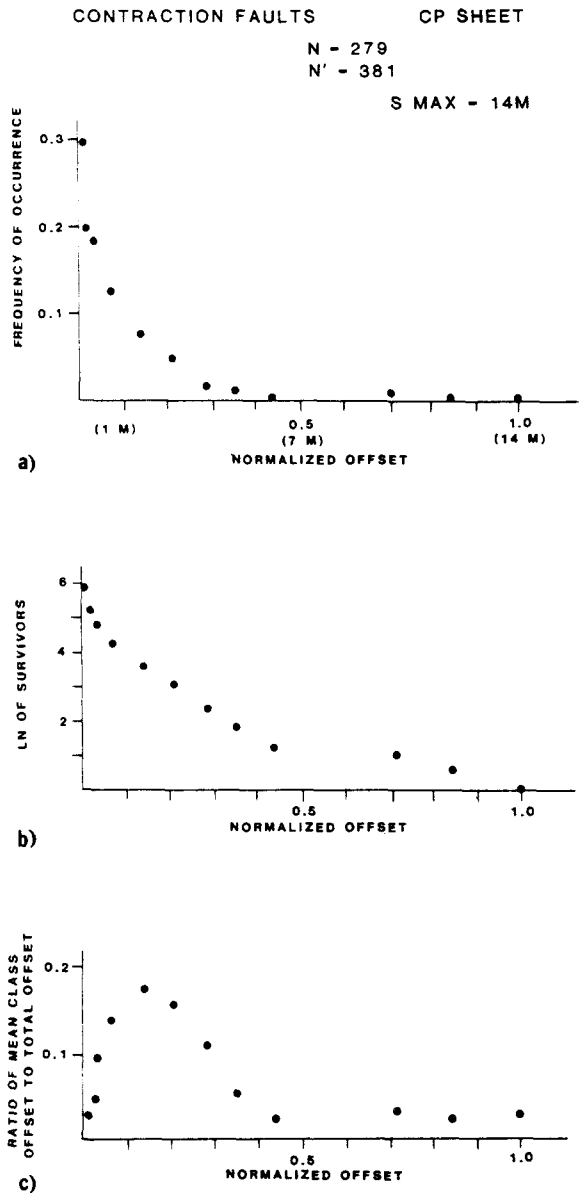

Fig. 12. (a) Distribution diagram for low-angle faults from deformed zone above CP thrust, derived from field observations, data from Fig. 4, and data from larger scale sections used to construct Fig. 4. (b) Survivorship curve for CP sheet low-angle faults. A survivorship curve is a plot of the logarithm of the number of individuals that survive to a particular age (size) vs age (size); its slope corresponds to the mortality rate. A concave upwards survivorship curve indicates that mortality rate decreases with age; a concave downwards survivorship curve indicates that mortality rate increases with age. (c) Plot of S_i/S_t values vs normalized offset for low-angle faults in CP sheet.

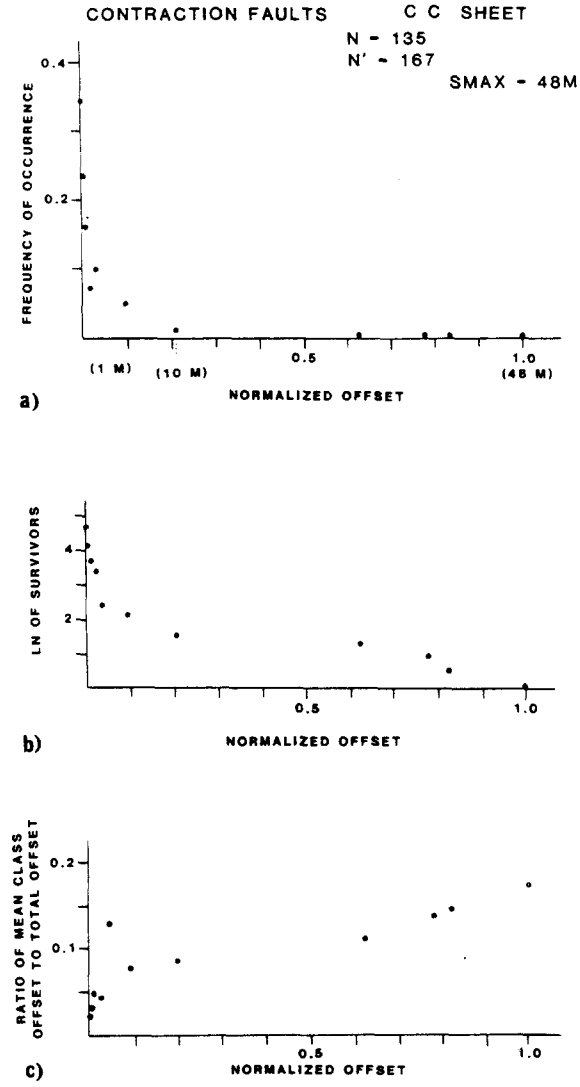

Fig. 13. (a) Distribution diagram for low-angle faults from deformed zone above CC thrust, derived from field observations, data from Fig. 6, and data from larger-scale sections used to construct Fig. 6. (b) Survivorship curve for CC sheet low-angle faults. (c) Plot of S_i/S_t values vs normalized offset for CC sheet low-angle faults.

by the ratio S_i/S_t. Plots of S_i/S_t vs normalized offset for low-angle faults in the CP and CC provide further support for the inferences on fault population dynamics. Small-offset faults occur most frequently in the CP sheet, but faults with offsets of 1 to 4 m account for almost 60% of the total observed offset (Fig. 11c). Faults with offsets $\geq$2 m account for the largest fraction of the total observed offset in the CC sheet (Fig. 13c).

The bimodal size distribution for low-angle faults in the CC sheet has implications for the dynamics of fault development in that sheet. Hallam (1972) stated that polymodality in the size distribution of a death assemblage occurs only if polymodality is present in the size distribution of the living assemblage. Polymodal size distributions occur in paleontology where recruitment is limited to specific periods of time or where an increase in the mortality rate coincides with a period of low growth rate. Either situation could apply to a dynamic fault population. It is likely that the rate of fault initiation will increase when a thrust sheet encounters an obstacle during its movement. In this case, processes such as the initiation of sheet movement or movement over a footwall ramp could bring about an increase in the rate of fault initiation. This new batch of 'recruits' might then be subjected to a set of dynamic parameters in which growth rates are initially low but increase as offset increases and the rates of cessation of activity decrease as offset increases. Alternatively, an increase in the rate of cessation of activity and a decrease in the slip rate could be associated with the glide of a sheet. The CC sheet negotiated a major footwall during its emplacement (Fig. 2b). This could have produced surges in the rate of minor-fault initiation during the initiation of

sheet movement and during movement over the footwall ramp, or it could provide for periods of increased cessation of activity and decreased slip rate on minor faults during each period of glide on a subhorizontal thrust.

Due to the quality of the exposure at the base of the HV sheet, an analysis of the population of low-angle faults from the HV sheet could not be completed. Likewise, difficulties in accurately estimating displacements on sufficient numbers of high-angle or bedding-parallel faults preclude this type of analysis for those components of minor-fault arrays. Qualitative results for high-angle faults, derived by assessing the relative numbers of large offset and small offset high-angle faults suggest that such an analysis would yield similar results.

It is unlikely that these statistics are biased by problems of preservation, a factor that paleontologists studying size distributions must consider, but possible sources of error deserve mention. Recognizing faults becomes harder as their displacements decrease. Field work for this study was completed with the view that all recognizable features in these rocks contribute to their deformation; considerable care was taken to record every fault recognized. Nevertheless, small-displacement faults may have been missed. If Figs. 12(a) and 13(a) are in error, it is likely that they underestimate the numbers of faults with small displacements. The 'true' populations might be more strongly skewed toward faults with small offset than indicated by Figs. 12(a) and 13(a). If this were true, inferences on the relative rates of attrition and 'growth' would have a stronger basis. On the other hand, this error could alter conclusions on the relative importance of faults in particular offset classes. The total observed offset in both the CP sheet and the CC sheet is (after correcting for sample areas of equal size) at least 250 m. In order to significantly change inferences on the relative importance of particular offset classes, small-offset faults would have to account for about 10% of this figure. Something of the order of 250 faults with 10 cm offsets would have to have been missed. When this number is compared to the total number of faults with 10 cm offsets that were recognized during careful work (of the order of 100–150) it seems that values in Figs. 12(c) and 13(c) may not be far from the actual values. This problem is exacerbated as displacement on faults decreases, though. Rocks within 10 m of the thrusts are cut by numerous microfaults; they might locally make a significant contribution to the total observed offset. Since microfaults are relatively rare in the remainder of these sheets, I feel that their effect can also be discounted. Finally, as cited earlier, Cooper *et al.* (1983) showed that a sizeable fraction of the bulk shortening of faulted strata occurred without leaving a record in the rock; they suggested that grain-boundary sliding or non-plane strain might account for this 'ghost' strain. The three sheets described here have suffered non-plane strain (Fig. 9). The net effects of missed faults, microfaults and other unrecognized deformation mechanisms must diminish the accuracy of the determinations of the relative importance of large offset faults. With this caveat in mind, I will proceed with examining the nature of the *observed* deformation in these rocks. Despite its shortcomings, this analysis raises some interesting points that are likely to apply to much of the deformed rock near these thrusts.

The low-angle fault populations in the CP and CC sheets are not identical, nor are they statistically distinct (Wojtal 1982). In both sheets, small-offset (displacement) faults are far more common than large-offset (displacement) faults, yet the large-offset faults account for more of the total observed offset. Survivorship curves (Figs. 12b and 13b) indicate that once low-angle faults in either sheet 'grew' to a certain displacement value, they were likely to remain active. This, in turn, suggests that the collection of low-angle faults in the CC sheet could have developed from a collection of low-angle faults like that in the CP sheet provided that large-offset faults continued to grow, accompanied by an on-going cycle of minor-fault initiation, continued activity, and cessation of activity under a set of dynamic parameters roughly equivalent to those that prevailed during the onset of deformation. This need not have been the case. For example, the relative rates of accumulation of displacement on faults with large and small displacements could change during progressive deformation, yielding distribution diagrams and survivorship curves with different shapes in far-traveled sheets. Their similarity suggests that the dynamic parameters reflect some fundamental characteristic of the deformation in foreland sheets.

This inference is supported by minor-fault S/V data. Faults with large offset (displacement) form an intersecting array and divide the base of each sheet into fault-bound blocks. Much of the deformation occurred by moving these blocks relative to their neighbors (Figs. 12c and 13c). Deformation in these sheets is similar to a large-scale 'grain-boundary' sliding, where smaller-offset faults within 'grains' accommodate 'grain-boundary' sliding. While there is no one-to-one correspondence between fault size and the magnitude of displacement on the fault, large faults are generally large-displacement faults. Clearly, a fault with a displacement of 1 m must be at least 1 m long. The relative magnitudes of S/V measurements for faults with observed lengths ≥ 1 m, then, give an indication of the size of the 'grains'. The larger the S/V measure for the fault, the smaller the 'grain' size. In the CP sheet, the tendency to distribute displacement among a small fraction of the total number of faults is well established (Fig. 12). Locally inhomogeneous deformation is the rule early in a sheet's history. The S/V value for faults at the base of this sheet is about 1.0 m^{-1}. In the CC sheet, the tendency to distribute displacement among a small fraction of the total number of faults is more highly exaggerated, yet the S/V value for faults at the base of this sheet is still about 1.0 m^{-1}. Rather than initiating new faults which could accumulate sufficient displacement to become significant contributors to the total observed offset, deformation proceeded by utilizing existing faults. This is apparent in the CC sheet's distribution diagram (Fig. 13) and its S/V values (Fig. 6). Deformation in the CC sheet is also locally inhomo-

geneous, but it is more inhomogeneous than that in the CP sheet.

The deformed zone at the base of the CP sheet is about 100 m thick. The deformed zones adjacent to the CC and HV thrusts are each 300–400 m thick. At the base of the CP sheet, there is a zone 10 m thick where the S/V value is about 1.0 m^{-1}. At the base of the HV sheet, there is a zone about 60–100 m thick where the S/V value is about 1.0 m^{-1}. At all places in these sheets, one finds the same sequence of minor faults. Combining these observations yields a picture of deformation in these sheets where there is a progressive thickening during sheet movement of the zone of highly deformed rock with high S/V values (Fig. 10). At all stages, the minor-fault populations developed under conditions which (1) favored an initially high attrition rate and slow 'growth' rate for minor faults and (2) favored the continued activity of minor faults and brought about a relative increase in their growth rate once they reached a certain displacement value. The approximately equal maximum values of fault S/V and the apparent thickening of deformed packages at the bases of sheets with continued deformation suggest that this type of deformation is accompanied by strain hardening (Wojtal & Mitra 1983 and in review).

STRAIN DUE TO MESOSCOPIC FAULTS

If the strain due to minor faults could be measured, the bulk deformation near these thrusts could be compared with that near thrusts in different geologic settings. In order to measure strain, deformation must be locally homogeneous. The discontinuous deformation near the CP, CC and HV thrusts is inhomogenous at any scale from a thin section to an individual outcrop. The conditions normally used to verify homogeneity, that material lines straight before deformation are straight after deformation, material lines parallel before deformation are parallel after deformation, and all material lines with a common orientation experience the same change in length (Ramsay 1967, pp. 50–54), are violated. A more fundamental criterion for homogeneous deformation, however, is that local values of displacement gradients are constant (Ramsay & Graham 1970). Movement on faults in a systematic array may give rise to displacement gradients that are roughly constant at a scale larger than the individual minor faults. In that case, deformation would be statistically homogeneous (Paterson & Weiss 1961). Once values of the displacement gradients in a statistically homogeneous deformation are measured, any of the common strain measures can be calculated from them.

Displacement gradients can be estimated if the displacements of discrete material points (measured with respect to the deformed state) are known as functions of their positions in the deformed state. In rock cut by a collection of minor faults, one systematic way to do this is to use a displacement diagram (Wojtal 1982 and in prep.). This is a graphical technique for determining the net displacements of discrete material points relative to a local material origin. For each set of material points in a deformed rock, there is a corresponding set of points on the displacement diagram. The line between the origin and any point on the displacement diagram is parallel to the displacement of the corresponding material point relative to the material origin; the line's length is proportional to the magnitude of the displacement of that material point relative to the material origin. The positions of material points relative to the material origin are known, so the displacements of material points relative to the local origin, u', can be determined as a function of their positions with respect to that origin, x'. Displacement differences, $\Delta u'/\Delta x'$, can be determined graphically or by calculation (Wojtal 1982 and in prep.). Measured values of the displacement differences, $\Delta u'/\Delta x'$, approximate local values of the displacement gradients, $\partial u'/\partial x'$, so any common strain measure can be calculated from $\Delta u'/\Delta x'$ values. This technique is best suited to analyzing two-dimensional deformations, but three-dimensional strains can be determined if the plane of analysis is a principal plane and the volume change during deformation is known.

This method was applied to rock at the base of the CP, CC and HV sheets using Figs. 4, 6 and 8. Since those figures are drawn parallel to local symmetry planes for mesoscopic deformation, the sections were assumed to be principal sections. Finite strains due to minor faults could be measured only in the CP sheet since displacement gradients in that sheet alone are constant at the scale of Figs. 4, 6 and 8.

Figure 14 is a displacement diagram constructed for all faults in the 10 m thick region immediately adjacent to the CP thrust. Reciprocal quadratic elongations calculated from measured displacement differences are the basis of a Mohr diagram for strain caused by minor faults in this layer (Fig. 15). It shows that the line of maximum shortening of material in the plane of section is oriented at a high angle (~60°) to the thrust surface and inclined to the W; the line of maximum elongation of material in the plane of section is inclined at ~30° to the thrust. The calculated ratio of final area in the plane of section to original area in the plane of section is 0.68. There is no evidence for large-scale removal of material from this region, so an assumption of constant volume during deformation is reasonable. With this assumption, it is possible to determine the three principal strain values for the deformation due to movement on minor faults in this region. The results indicate that material is predominantly flattened, $\nu \simeq 0.58$, with the maximum elongation in the plane of section (subparallel to transport). It is noteworthy that a significant volume of material moved out of the plane of the section; deformation is not plane strain. Deformation intensity is high. The logarithmic unit shear, $\bar{\varepsilon}_s$, has a value of about 1.5 in this region.

The overlying material was divided into five smaller areas in which strains were measured. Displacement diagrams (Fig. 16) and Mohr diagrams (Fig. 17) show a relatively smooth variation in deformation with distance from the thrust. Maximum shortening in the area closest

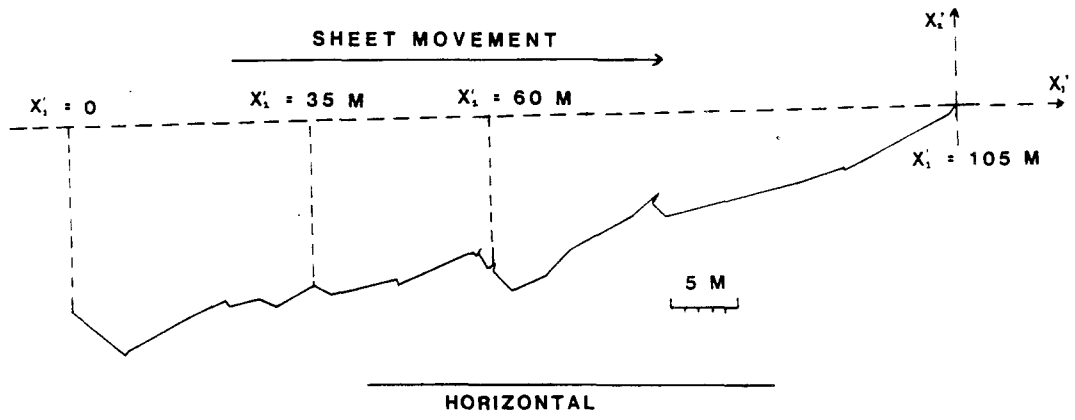

Fig. 14. Displacement diagram for all faults in 10 m thick layer at base of CP sheet. All displacement and position vectors are measured with respect to the deformed state, i.e. using an Eulerian specification (Ramsay & Graham 1970). The displacement of any fault-bound block with respect to its nearest neighbor is taken to be the offset on the fault which separates those blocks; the effects of internal distortion of blocks are ignored. The diagram portrays net displacements of blocks relative to an arbitrarily chosen origin in one block in the manner described in the text. The net displacement of a fault-bound block one block removed from the origin is the resultant of its displacement relative to its nearest neighbor and its nearest neighbor's displacement relative to the origin. The net displacement of any block relative to the origin is the resultant of the displacements of nearest neighbors along a line between that block and the arbitrary origin. Fault-bound blocks chosen for the diagram lie along a line parallel to the thrust (x'_2 is constant for all blocks); blocks at different positions along this line (e.g. $x'_1 = 35$ m, $x'_1 = 60$ m) have the net displacements indicated on the diagram.

to the thrust (area I) occurred along a line inclined about 55°W relative to the thrust; maximum elongation in this plane is inclined about 35°E relative to the thrust. The ratio of area in the deformed section to initial area for this area is about 0.80. Assuming constant material volume during deformation, the logarithmic unit shear, $\bar{\varepsilon}_s = 0.8$ and $\nu \simeq 0.6$, with the maximum elongation laying in the plane of section. Material is again flattened subparallel to the underlying thrust. The overlying areas (areas II, III, IV and V) exhibit similar deformation patterns. Area II has maximum shortening along a line inclined 60°W relative to the thrust surface and maximum elongation inclined 30°E relative to the thrust in this plane. Assuming constant volume, $\nu \simeq -0.02$, and $\bar{\varepsilon}_s = 0.30$. Maximum shortening in area III is inclined about 45°W relative to the thrust and maximum elongation about 45°E relative to the thrust surface. With constant volume, $\nu \simeq -0.08$, and $\bar{\varepsilon}_s = 0.34$. Area IV has maximum shortening inclined about 45°W and maximum elongation about 45°E relative to the thrust surface. $\nu = -0.57$, and $\bar{\varepsilon}_s = 0.35$ if there was no volume change. In area V, the principal directions are again inclined about 45° to the thrust. $\nu \simeq -0.8$, and $\bar{\varepsilon}_s = 0.2$ if volume did not change during deformation. The appar-

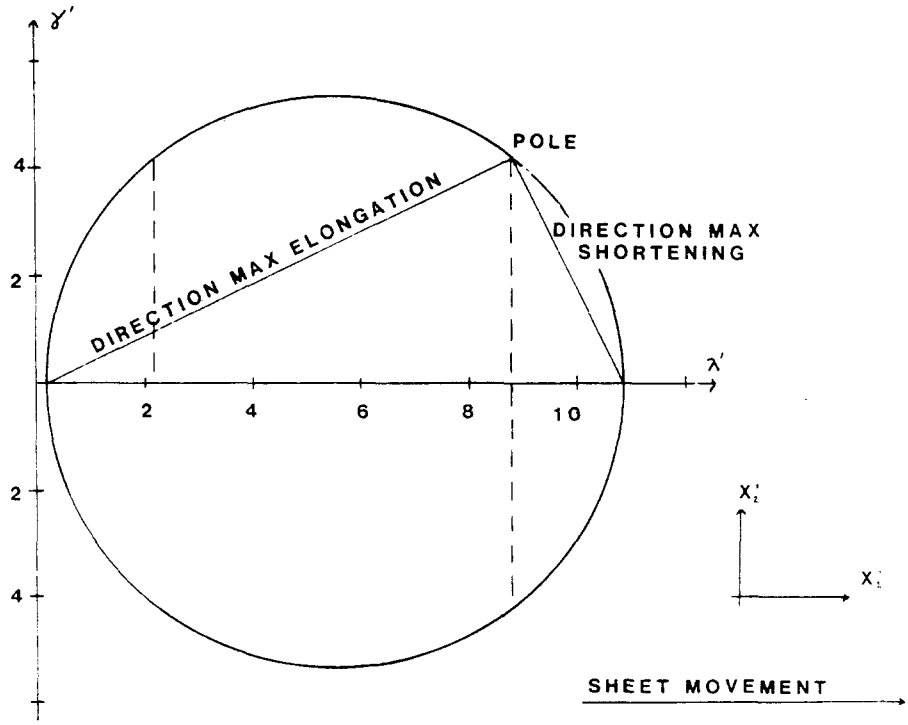

Fig. 15. Mohr diagram for strain in 10 m thick layer at base of CP sheet.

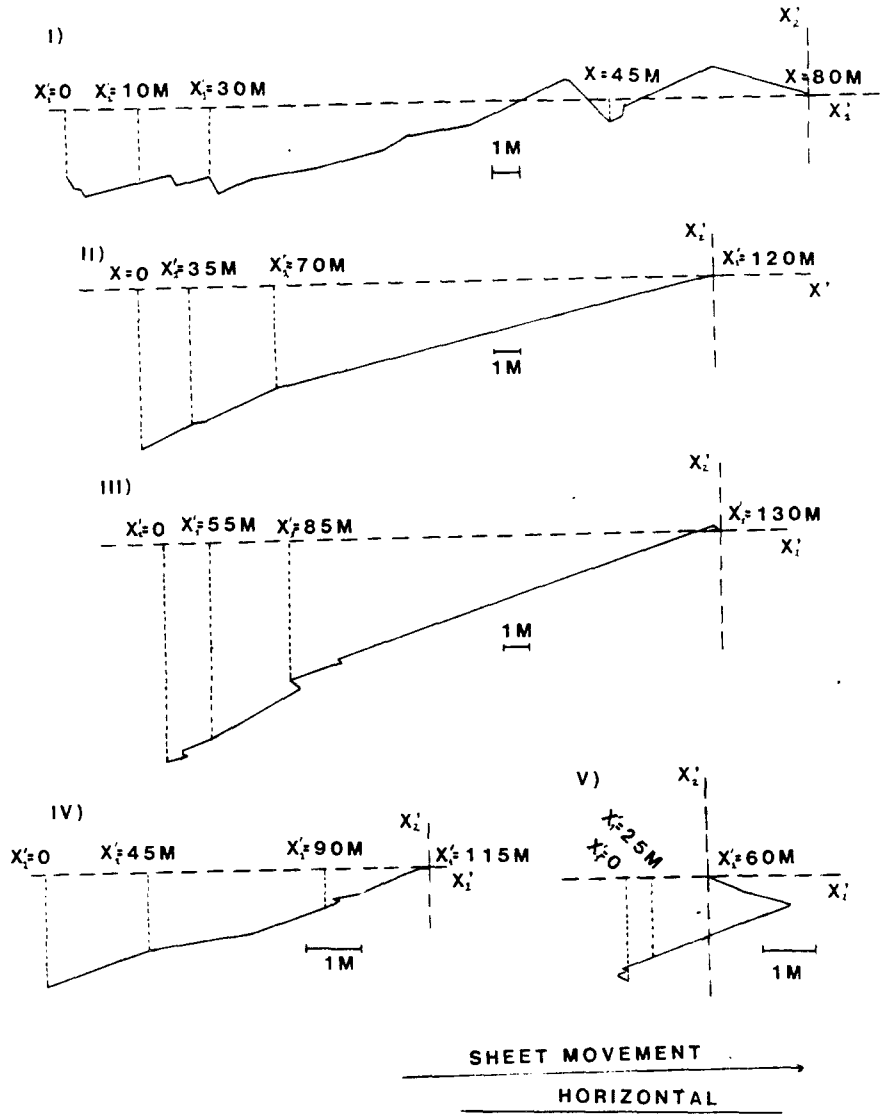

Fig. 16. Displacement diagrams for all faults from five smaller areas in central part of deformed zone above CP thrust. Diagrams are plotted in the manner described in the caption to Fig. 14.

ent constriction ($\nu < 0$) in this part of the sheet may be due to errors in strain measurements. Strains in these areas are very low, and calculated area ratios are about 1.1:1. Such low strains may not be within the resolution of this strain measurement technique. In fact, the extension normal to transport seen near the thrust must affect this part of the sheet if strains are to be compatible. I saw no evidence for movement normal to transport in these areas other than that described in Fig. 9. The map-scale transverse extension faults seen in foreland sheets might account for this lateral extension without affecting outcrop-scale features.

Although the mirror plane for mesoscopic deformation in the sandstones and conglomerates at the top of the deformed zone above the CP sheet parallels that in the underlying rock, the directions of maximum shortening and elongation are quite different. Maximum elongation in the plane of section is inclined about 30°W relative to the thrust; it dips in the direction of transport (Fig. 18). Strains in this part of the sheet may reflect a sort of 'outer arc' extension as strata draped over the thickened package below (Wojtal 1982). This region has $\bar{\varepsilon}_s = 0.16$ and $\nu \simeq -0.18$ if there was no volume change during deformation.

The overall pattern to deformation near the CP thrust is similar to that observed near thrusts in other geological settings. Deformation intensity is greatest near the thrust and decreases markedly with increasing distance from the thrust (Fig. 19). Calculated axial ratios in the plane of section vary from about 7:1 near the thrust to about 1.5:1 only 50 m from the thrust. The attitudes of the principal directions of strain in the plane of section vary systematically with distance from the thrust. Nearest the thrust, maximum elongation is inclined at a low angle (~30°E) to the thrust surface; farther from the thrust, maximum elongation is more upright. Had cleavage developed in this sheet in response to equivalent strains, the attitudes of cleavage would mirror those observed near other thrusts (Boyer 1978, Mitra & Elliott 1980, Kumpulainen 1980). I suspect that strain principal directions would asymptotically approach the thrust if strains could be measured at a finer scale. Finally,

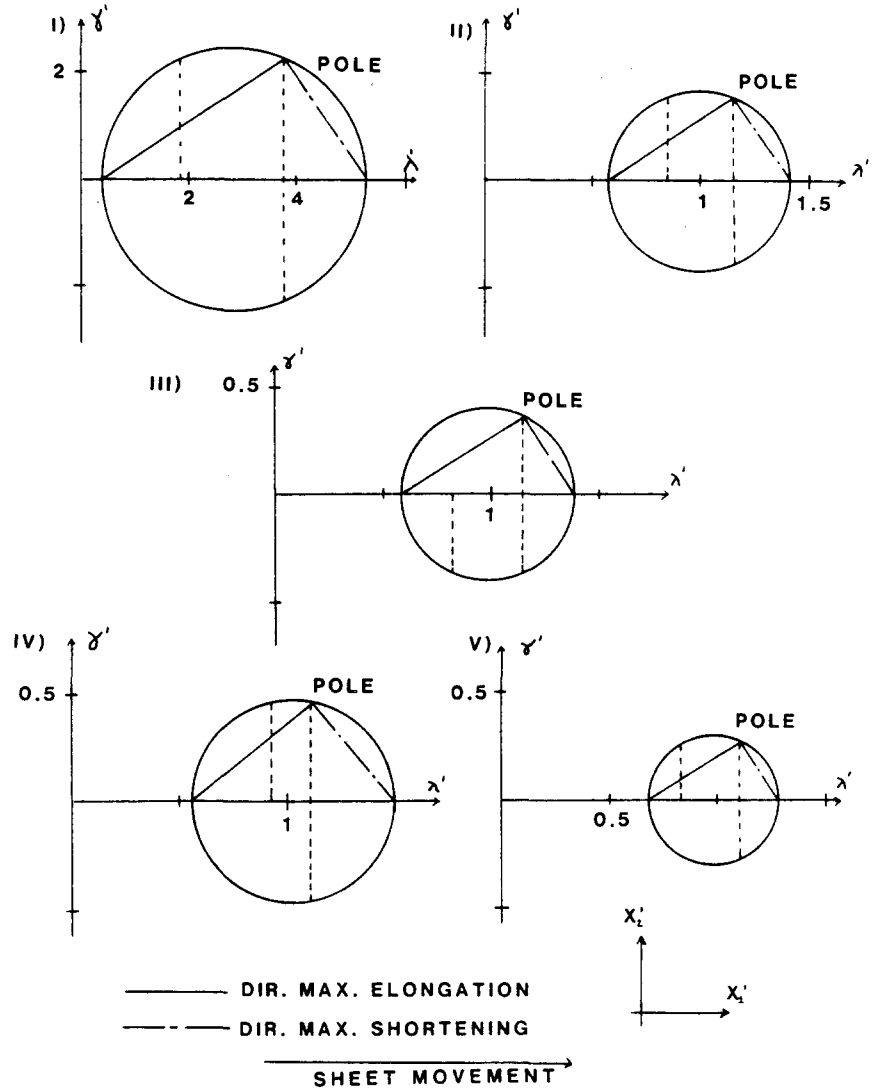

Fig. 17. Mohr diagrams for five areas in central portion of deformed zone above CP thrust.

deformation near the thrust is demonstrably non-plane strain. This too is similar to observations near other thrusts (Chapman *et al.* 1979, Sanderson *et al.* 1980, Allmendinger 1982). The strain measurements support the arguments for non-plane strain made earlier on more qualitative grounds; they also suggest that comparable effects can be expected in the CC and HV sheets.

CONCLUSIONS

Despite differences in their lithological composition, their individual tectonic histories, and their overall location in the thrust belt, the three Appalachian thrust sheets described in detail exhibit a single style and pattern in their deformation. Penetrative cleavage is not observed in any of the sheets, nor can whole-rock homogeneous strain be demonstrated to be an important contributor to deformation throughout these sheets. At any scale from that of a hand sample to that of an individual outcrop, deformation is discontinuous and inhomogeneous. The deformation in each is a product of relative motion of largely undeformed blocks of rock on discrete minor faults, essentially a very coarse-scale 'grain-boundary' sliding. Minor fault populations in these sheets are comparable in their geometry and internal distribution of displacement.

With regard to their geometry, a plane that is both perpendicular to the thrust and parallel to sheet transport is a plane of mirror symmetry for the mesoscopic deformation of each sheet. Mesoscopic deformation in each sheet records a strong sense of movement of structurally higher portions of the sheet further toward the craton; deformation has a strong rotational or simple shear component. This shearing occurred in two stages. Rock was first shortened subparallel to transport and thickened by low-angle faults. It was later extended both subparallel and normal to transport and thinned by high-angle faults. This deformation sequence is locally seen where high-angle faults cut across low-angle faults, and it is preserved in profiles normal to each thrust, where rock that has been shortened and thickened only overlies rock first shortened and thickened and then flattened and extended. This sequence is also apparent in comparisons between the far-traveled CC and HV sheets and the CP sheet; the entire layer of deformed

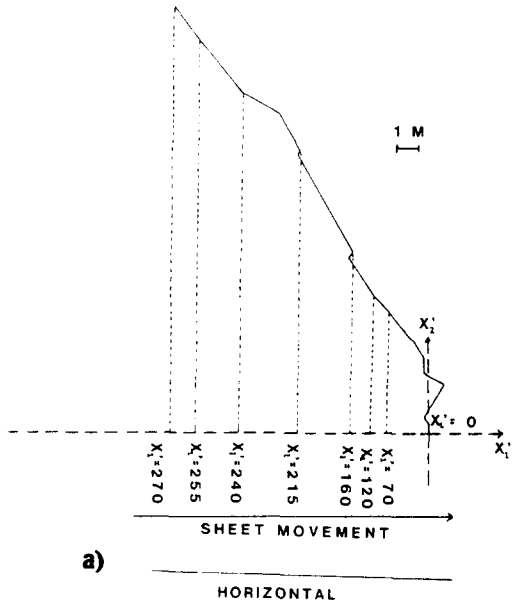

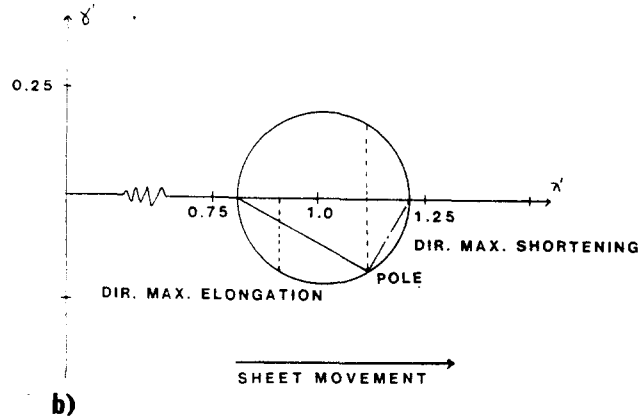

Fig. 18. (a) Displacement diagram for upper portion of deformed zone above CP thrust. Diagram plotted in the manner described in the caption to Fig. 14. (b) Mohr diagram for strain in upper portion of deformed zone above CP thrust.

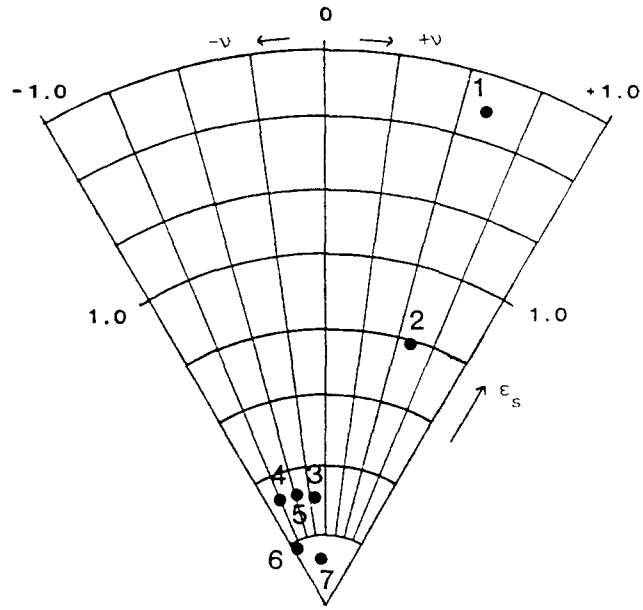

Fig. 19. Hsu plot for measured strains above CP thrust. 1, 10 m thick layer at base; 2–6, five smaller areas in central portion—2 closest to thrust, 6 furthest from thrust; 7, upper portion of deformed zone.

rock at the base of the far-traveled sheets is thicker in the CC and HV sheets than in the CP sheet, as are each of its components. Movement on a thrust appears to have been accompanied by a progressive thickening of the deformed zone adjacent to the thrust. There is also evidence in these sheets for the diverging flow inferred by Bielenstein (1969); displacement on nearly all individual components of the minor-fault arrays provided for movement normal to transport during deformation.

In regards to the distribution of displacement among minor faults, conditions favoring high attrition rates and relatively slow growth for small-displacement faults, and lower attrition rates and faster growth for faults with larger displacements persisted throughout emplacement. In the CC and HV sheets, where these conditions presumably persisted for longer time periods, the deformation is inhomogeneous at a scale larger than individual minor faults. In the CP sheet, where these conditions presumably did not persist for a long time period, the deformation is demonstrably homogeneous at a scale larger than individual minor faults. Strains due to this mesoscopic deformation in the CP sheet are similar to those in sheets emplaced in different geologic settings. Bulk deformation in thrust sheets is remarkably similar despite the differences in the way in which this deformation is accomplished.

Acknowledgements—Much of the work for this paper was completed while I was a doctoral student under David Elliott. His insight and encouragement is gratefully acknowledged; it is sorely missed. I am also grateful to fellow graduate students at Johns Hopkins for their comments. Thoughtful reviews by David Sanderson and an anonymous referee significantly improved this manuscript.

REFERENCES

Allmendinger, R. W. 1982. Analysis of microstructures in the Meade plate of the Idaho–Wyoming foreland thrust belt, U.S.A. *Tectonophysics* **85**, 221–251.

Beach, A. 1982. Strain analysis in a cover thrust zone, external French Alps. *Tectonophysics* **88**, 333–346.

Bielenstein, H. U. 1969. The Rundle thrust sheet, Banff, Alberta: Ph.D. dissertation, Queen's University, Kingston, Ontario.

Boyer, S. E. 1978. Structure and origin of Grandfather Mountain Window, North Carolina. Ph.D. dissertation, Johns Hopkins University, Baltimore, Maryland.

Boyer, S. E. & Elliott, D. 1982. Thrust systems. *Bull. Am. Ass. Petrol. Geol.* **66**, 1196–1230.

Bryant, B. & Reed, J. C., Jr. 1969. Significance of lineation and minor folds near major thrust faults in the southern Appalachians and the British and Norwegian Caledonides. *Geol. Mag.* **106**, 412–429.

Chapman, T. J., Milton, N. J. & Williams, G. D. 1979. Shape fabric variations in deformed conglomerates at the base of the Laksefjord Nappe, Norway. *J. Geol. Soc. Lond.* **136**, 683–691.

Cooper, M. A., Garton, M. R. & Hossack, J. R. 1983. The origin of the Basse Normandie duplex, Boulonnais, France. *J. Struct. Geol.* **5**, 139–153.

Craig, G. Y. & Oertel, G. 1966. Deterministic models of living and fossil populations of animals. *J. Geol. Soc. Lond.* **122**, 315–355.

Diegel, F. A. & Wojtal, S. F. 1985. Structural transect in SW Virginia and NE Tennessee. In *Field Trips in the Southern Appalachians* (edited by Woodward, N. B.), Univ. of Tennessee, Dept. of Geological Sci. *Studies in Geology* **9**, 70–143.

Durney, D. W. & Ramsay, J. G. 1973. Incremental strains measured by syntectonic crystal growth. In: *Gravity and Tectonics* (edited by De Jong, K. A. & Scholten, R.), Wiley, New York, 67–96.

Elliott, D. 1976. The energy balance and deformation mechanisms of thrust sheets. *Phil. Trans. R. Soc.* **A283**, 289–312.

Elliott, D. 1977. Some aspects of the geometry and mechanics of thrust belts. Lecture Notes to 8th Annual Can. Soc. Pet. Geol. Seminar, Calgary, Alberta, Vol. 1.

Groshong, R. H. 1972. Strain calculated from twinning in calcite. *Bull. geol. Soc. Am.* **83**, 2025–2038.

Groshong, R. H., Pfiffner, O. A. & Pringle, L. R. 1984. Strain partitioning in the Helvetic thrust belt of eastern Switzerland from leading edge to the internal zone. *J. Struct. Geol.* **6**, 19–32.

Hallam, A. 1972. Models involving population dynamics. In: *Models in Paleoecology* (edited by Schopf, T. J.), Freeman, Cooper and Co., San Francisco, 62–80.

Hansen, E. 1967. A method of deducing slip-line orientations from the geometry of folds. *Carnegie Inst. Yb.* **65**, 387–405.

Harris, L. D. & Milici, R. C. 1977. Characteristics of thin-skinned style of deformation in the southern Appalachians and potential hydrocarbon traps. *Prof. Pap. U.S. geol. Surv.* **1018**, 1–40.

Kumpulainen, R. 1980. Upper Proterozoic stratigraphy and depositional environments of the Tossasfjället Group Särv Nappe, southern Swedish Caledonides. *Geol. För. Stockh. Förh.* **102**, 531–550.

Kvale, A. 1953. Linear structures and their relation to movement in the Caledonides of Scandinavia and Scotland. *J. geol. Soc. Lond.* **109**, 51–74.

Milici, R. C. 1963. Low-angle overthrust faulting as illustrated by the Cumberland Plateau–Sequatchie Valley Fault System. *Am. J. Sci.* **261**, 815–825.

Mitra, G. & Elliott, D. 1980. Deformation of basement in the Blue Ridge and the development of the South Mountain cleavage. In: *The Caledonides in the U.S.A.* (edited by Wones, D. R.), Dept. of Geological Sciences, V.P.I. and S. U. Mem. **2**, 307–311.

Nadai, A. 1963. *Theory of Flow and Fracture of Solids*, Vol. II. McGraw-Hill, New York, 1–705.

Norris, D. K. 1958. Structural conditions in Canadian coal mines. *Bull. geol. Surv. Can.* **44**, 1–54.

Paterson, M. S. & Weiss, L. E. 1961. Symmetry concepts in the structural analysis of deformed rocks. *Bull. geol. Soc. Am.* **72**, 841–887.

Price, R. A. 1967. The tectonic significance of mesoscopic subfabrics in the southern Rocky Mountains of Alberta and British Columbia. *Can. J. Earth Sci.* **4**, 39–70.

Ramsay, J. G. 1967. *Folding and Fracturing of Rocks*. McGraw-Hill, New York, 1–568.

Ramsay, J. G. 1974. Development of chevron folds. *Bull. geol. Soc. Am.* **85**, 1741–1754.

Ramsay, J. G. & Graham, R. H. 1970. Strain variation in shear belts. *Can. J. Earth Sci.* **7**, 786–813.

Reches, Z. 1978. Analysis of faulting in a three-dimensional strain field. *Tectonophysics* **47**, 109–129.

Reks, I. J. & Gray, D. R. 1983. Strain patterns and shortening in a folded thrust sheet: an example from the southern Appalachians. *Tectonophysics* **91**, 99–128.

Rodgers, J. 1970. *The Tectonics of the Appalachians*. Interscience, New York, 1–271.

Roeder, D., Gilbert, O. E., Jr. & Witherspoon, W. D. 1978. Evolution and macroscopic structure of Valley and Ridge Province thrust belt, Tennessee and Virginia. Univ. of Tennessee, Dept. of Geological Sci. *Studies in Geology* **2**, 1–25.

Sanderson, D. J. 1973. The development of fold axes oblique to the regional trend. *Tectonophysics* **16**, 55–70.

Sanderson, D. J., Andrews, J. R., Phillips, W. E. A. & Hutton, D. H. W. 1980. Deformation studies in the Irish Caledonides. *J. Geol. Soc. Lond.* **137**, 289–302.

Simon, R. I. & Gray, D. R. 1981. Interrelations of mesoscopic structures and strain across a small regional fold, Virginia Appalachians. *J. Struct. Geol.* **4**, 271–289.

Spang, J. H. & Brown, S. P. 1981. Dynamic analysis of small imbricate thrust and related structures, Front Ranges, Southern Canadian Rocky Mountains. In: *Thrust and Nappe Tectonics* (edited by McClay, K. R. & Price, N. J.). *Spec. Publs geol. Soc. Lond.* **9**, 143–151.

Turner, F. J. & Weiss, L. E. 1963. *Structural Analysis of Metamorphic Tectonites*. McGraw-Hill, New York.

Underwood, E. E. 1970. *Quantitative Stereology*. Addison-Wesley, Reading, MA, 1–274.

Williams, G. D. 1976. Rotation of contemporary folds into the X-direction during overthrust processes in Laksefjord, Finmark. *Tectonophysics* **48**, 28–40.

Wiltschko, D. V., Medeweff, D. A. & Millson, H. E. 1985. Distribution and mechanisms of strain within rocks on the northwest ramp of the Pine Mountain block, Southern Appalachian foreland. *Bull. geol. Soc. Am.* **96**, 426–435.

Wojtal, S. F. 1982. Finite deformation in thrust sheets and their material properties. Ph.D. dissertation, Johns Hopkins University, Baltimore, Maryland.

Wojtal, S. & Mitra, G. 1983. Strain hardening by mesoscopic deformation during emplacement of foreland thrust sheets. *Geol. Soc. Am. Abstr. With Progr.* **15**, 722.

Wojtal, S. & Mitra, G. In review. Strain hardening and strain softening in fault zones from foreland thrusts. *Bull. geol. Soc. Am.*